Morphological and rheological properties of polypropylene filled with synergistic combinations of sorbitol, POSS and carbon nanotubes

Research report

by

Hannelore Isabella Mattausch, M.Sc.

December 2012

ABSTRACT

The use of polypropylene (PP) nanocomposites has attracted significant academic and industrial interest over the last years. The main advantage of these nanofillers in the polymer matrix, compared to conventional micro-scaled fillers, is the significant smaller amounts of filler need to enhance properties (e.g. Young's modulus) or to establish a multifunctional property profile. Carbon nanotubes (CNT) have exceptional thermal, mechanical and electrical properties.

CNT are allotropes of carbon with a cylindrical structure and are categorized as single-walled nanotubes and multi-walled nanotubes. Polyhedral oligomeric silsesquioxance (POSS) as nanofiller leads to greater temperature and oxidation resistance, surface hardening and reduction in flammability.

But there are still many challenges that must be analyzed to reach the full potential of the polymer nanocomposites (PNC). To reach this good performance a homogeneous dispersion of the nanofillers in the polymer matrix, strong interfacial adhesion between the nanofillers and the polymer matrix and synergistic combinations of various nanofillers are needed. The property enhancements correlate strongly with the morphology of the polymer nanocomposite. So it is necessary to characterize the microstructure of these materials in order to establish adequate structure-property relationships.

Wide-angle X-ray diffraction (WAXD) can provide insight into the orientation factors and the apparent crystallinity of polymer nanocomposites. The scanning electron microscope (SEM) and transmission electron microscope (TEM) is a good method to investigate the morphology of the PNC. Rheological measurements can be a powerful tool for fundamental insights about the state of dispersion because the rheological values (storage modulus G', loss modulus G'' and complex viscosity are sensitive to the dispersion of the dispersed phase. Further characterization methods such as differential scanning calorimeter (DSC), tensile tests, polarized cross microscope (POM) and X-ray photoelectron spectroscopy (XPS) will also be applied.

In this research work the focus is on the morphology and rheological properties of PP nanocomposites spun fibers filled with synergistic combinations of DBS, POSS and

nanofillers such as CNT, silica or nanosilicon. The viscosity of PP will be decreased using POSS and will be increased using CNTs. A synergistic combination will allow melt viscosity of the filled nanocomposites to be at par with the unfilled melt. The presences of these nanofillers are expected to alter the power-law index, frequency dependence of storage and loss modulus, possibly occurrence of slip. This research work will provide a deeper understanding of the structure-property relationships of PNCs, PNC fibers and their process dependency. To determine these structure-property relationships several analytical methods such as WAXD, SEM, TEM and rheological measurements will be applied on different combinations and concentrations of the nanofillers in the polymer matrix polypropylene. Furthermore additional benefit generated by the nanofiller interactions will be evaluated. Thereby the determination of interfacial properties and processes will lead to an in-depth understanding of the mode of operation of different sized, shaped and surface modified nanofiller and their combinations.

TABLE OF CONTENT

1 INTRODUCTION

Polypropylene nanocomposites (PNC) are in the focus of interest in many fields of possible applications. The reason is that polypropylene (PP) offers good performance in many different applications (automotive, biomedical components, home appliances) and a good cost-performance ratio [Onder et al. (2012); Karian (1999); Luyt et al. (2009)]. But this engineering material presents practical limitations such as low toughness, low service temperature and high flammability for many different applications [Onder et al. (2012); Wang et al. (2011)]. To overcome these disadvantages nanotechnology is taken as solution process.

The idea of nanoparticles exists as far back as several centuries. For example, Paracelsus described the preparation of gold nanoparticles dispersed in liquids around 1570 [Caseri (2000); Paracelsus and von Bodenstein (1563); von Hohenheim (1572)]. The use of silver nanoparticles was first mentioned in 1677 by Valentinus [Caseri (2000); Valentinus et al. (1677)]. These nano-scaled metal colloids were used as colored glasses. In literature the first polymer nanocomposite were mentioned in 1835 [Caseri (2000); Shepard (1835)] respectively in 1833 (the original abstract) [J. Erdmann (1833)]. Gold salt was reduced in the presence of gum-arabic in an aqueous solution; hence a purple solid nanocomposite was obtained by coprecipitation with ethanol [Caseri (2000); Shepard (1835)]. At the turn of the century, polymer nanocomposites with uniaxially oriented inorganic particles were produced with remarkable optical properties [Caseri (2000); Ambronn (1896); Ambronn (1899)].

The first commercial polymer nanocomposite was developed by Toyota researchers in the early 1990s and was based on polyamide (PA) 6 and layered silicates [Pavlidou and Papasrides (2008); Usuki et al. (1993); Usuki et al. (1995)]. Olefin nanocomposites filled with montmorillonite (MMT) was produced by General Motors and partners Basell, Southern Clay Products and Blackhawk Automotive Plastics first [Pavlidou and Papasrides (2008)].

Numbers of successful stories about the enhancement of special properties of polymer nanocomposites give evidence to the hypothesis that already a small

amount of nanofiller (< 5 wt %) are needed to get significant better performance of the material. To name but a few of the advantages of nanofilled polymer, some examples are listed.

A lot of research activities of polymer nanocomposites filled with organo-modified clay appeared which the most industrial used nanofiller are. Modified MMT can enhance thermal properties [Gilman (1999); Ray and Okamoto (2003)], mechanical properties [Gilman (1999); Hasegawa et. al (2000); Kojima et al. (1993); Giannelis (1996); Ray and Okamoto (2003)], protective barrier [Kashiwagi et al. (2004)], decreased gas permeability [Zanetti et al. (2001); Zhu et al. (2001); Alexandre et al. (2001)] and enhance the degradation rate of biodegradable polymer [Ray and Okamoto (2003]. Also in the topic of flame retardancy the layered silicate can achieve an improvement [Gilmann (1999); Marosi et al. (2003); Kashiwagi (2004); Ray and Okamoto (2003); Kiliaris and Papaspyrides (2010)].

Many studies have focused on anionic clays (MMT are cationic clays) with hydrotalcite like structure, which are called Layered Double Hydroxides (LDH) because of their ion exchange properties [Trifiro and Vaccari (1996); Rives (2001); Inayat et al. (2011); Leroux and Besse (2001)]. LDH particles enhance the thermal stability, mechanical properties and improve the flame retardancy properties [Ardanuy and Velasco (2011); Camino et al. (2001); Nyambo and Wilkie (2009); Nyambo et al. (2009); Manzi-Nshuti et al. (2009)].

Polyhedral oligomeric silsequioxanes (POSS) influences the thermal stability in a positive way, allows to tailoring of the polymer glass transition temperature and improves the fire resistance of the polymer nanocomposite [Fina et al. (2005); Zheng et al. (2002); Fasce et al. (1999); Sellinger and Laine (1996); Wu and Mather (2009)].

Carbon Nanotubes (CNT) are a highly effective flame retardants [Beyer (2002); Ma et al. (2007); Kashiwagi et al. (2002); Schartel et al. (2005)], have remarkable mechanical properties [Chang et al. (2005); Sandler et al. (1999); Haggenmueller et al. (2003); Iijima (1991); Prashantha et al. (2009)] and enhances the electrical [Valentino et al. (2008); Prashantha et al. (2008)] and thermal [Bikiaris et al. (2008) Prashantha et al. (2008)] properties.

Recently, graphene based nanocomposites have attracted the interest of scientists and industry. Graphene is regarded as the strongest material to date by theoretical

and experimental results. Graphene based nanocomposites improve simultaneously the mechanical properties and barrier properties as well as thermal properties or electronic transport properties [Song et al. (2011); Alzari et al. (2010); Lee et al. (2008); Kuilla et al. (2010)].

These positive examples for good performance of nanofillers in a polymer matrix are often due to the predominant interfacial interactions between the filler and the polymer matrix, which is facilitated by large area per unit volume [Lee (2009)]. Layered silicates have a surface area of about 760 m^2/g [Theng (1974); LeBaron et al. (1999); Ray and Okamoto (2003)], POSS of about 406 m^2/g [Lee (2009); Mantz et al. (1996)], single wall carbon nanotubes of about 400 m^2/g [Lee (2009); Esteves et al. (2009); Arai et al. (2007)] and multi wall carbon nanotubes of about 150 – 200 m^2/g [Peigney et al. (2001)].

For adequate interactions between the nanofiller and the polymer, the nanofillers have to be dispersed homogenously in the polymer matrix. But the dispersion of inorganic nanoparticles in the polymer matrix is often not easy possible. So the combination of the adequate processing technique, polymer-nanofiller interactions (good interfacial adhesion) and correct chemical modification method of the components is very important for reaching high dispersed polymer nanocomposites with a good property profile. Poor distribution can lead to agglomeration of the fillers in the matrix or prevent formation between the filler surface and the polymer matrix [(Vargas et al. (2010)]. Especially for non-polar polymers such as polypropylene or polyethylene the challenge is the homogenous dispersion of fillers in the polymer matrix. Maleic anhydride acid (MA), for instance, has been employed as important compatibilization agent for layered silicates. The MA adds polar moieties to the polymer chains in order to improve the interface interactions [Vargas et al. (2010)]. Another important factor for the performance of the material is the filler geometry. Scott et al. (2007) and Vlasveld et al. (2005) and their co-workers have found out that polyamide 6 composites filled with different filler shape and sizes showed different rheological behavior, which also depends on the aspect ratio of the used particles [Vargas et al. (2010); Scott et al. (2007); Vlasveld et al. (2005)].

The use of polymer nanocomposites in versatile applications has great potential and will increase in future dramatically. Therefore also the concerns about the public and

occupational exposure of nanoparticles to the environment will be a very important factor and the government and scientific communities give more attention towards safety aspects of nanomaterials. Nanotoxicology wants to understand the exposure and assessment of nanoparticles, transport and interaction process with the human body [Dreher (2004); Singh et al. (2011)]. For example, carbon nanotubes have huge potential exposure (by inflammatory and fibrotic reactions) to the environment and living systems [Muller et al. (2006)]. The work of several research groups has revealed that CNT could induce genotoxicity via induction of reactive oxygen species [Singh et al. (2011); Zhang et al. (2010); Lindberg et al. (2009)].

So the research of long term fate, health and environmental risk assessment of polymer nanocomposites is widely lacking. CNTs can also be a helpful material for medicine therefore the research in this topic should go on.

2 FUNDAMENTALS

In this chapter the main fundamentals about the materials and the processing are described. Nanoparticles can be classified by their dimensionality. According to this classification POSS are 0-dimensional nanoparticles, MWCNT 1-dimensional, layered silicates 2-dimensional while silica-nanoparticles (SiO_2) are 3-dimensional [Gyeong-Mang (2007)].

2.1 Polyhedral oligomeric silsesquioxane

Silsesquioxanes belong to the group o organo-silicium compounds and consist of a Si-O-Si network. Polyhedral oligomeric silsesquioxane (POSS) are cage-shaped compounds and embody a truly hybrid (inorganic-organic) architecture, which contains an inner inorganic framework made up of silicone and oxygen surrounded by organic substituents [Li et al. (2001)]. All structures of these 0-dimensional nanofillers have the empirical formula $(RSiO_{1.5})_n$, where R is an organic group or a hydrogen. Due to the variable combinations of Si atoms and possible organo-functionalization of the Si-O-Si network, there are a huge variety of types.

The development of POSS molecules started likely in the 1930's. Alkyltriethoxysilanes were formed in water by hydrolyzing, which were the first synthesis of those particles. Due to the lack of English publications his research work were not recognized by the scientific community [Andrianov (1938); Andrianov (1946); Matisons (2011)].

In 1946 the first oligomeric organo-silsesquioxanes were isolated by Scott through thermolysis of polymeric products obtain from methyl-tri-chloro-silane and di-methyl-chloro-silane cohydrolysis [Li et al. (2001), Scott (1946)].

Barrey and his co-workers made a lot of research regarding the structure, preparation, properties and applications of silsesquioxanes. The molecular structure of POSS was determined which were prepared by alkali-catalyzed siloxane rearrangement of organo-tri-chloro-silane hydrolyzates by single-cystral X-ray diffraction [Lee (2009); Barrey et al. (1955)].

Baney and his co-authors made a lot of research regarding the structure, preparation, properties and applications of silsesquioxanes and published in 1995 [Li et al. (2001)].

The interactions between POSS molecules and polymer matrices are still investigated insufficiently. Especially synergistic combinations with other fillers are neglected.

Nanocomposites containing non-reactive POSS are favorable due their processability by conventional melt compounding techniques [Lee (2009)]. During the standard extrusion process the chemical structure of non-reactive POSS may lead to the formation of agglomerates inside the polymer matrix. However it is easy to obtain a good compatibility and dispersion of POSS nanoparticles inside the polymer matrix but depending on the hierarchical morphology generated by processing [Lee (2009)].

Possible applications of these ladder-like silsesquioxane polymers are as photoresist coatings [Li et al. (2001); Gozdz (1994); Yoneda et al. (1982); Uchimura et al. (1983); Adachi et al. (1990); Adachi et al. (1985); Adachi et al. (1992)], for electronics and optical devices, liquid crystal display segments [Li et al. (2001); Shoji et al. (1981); Azuma et al. (1982)], magnetic recording media [Imai and Takeno (1984); Yanagisawa (1987)], optical fiber coatings [Mishima and Nishimoto (1992)], gas separation membranes [Saito et al. (1983); Mi and Stern (1991)], binders for ceramics [Mine and Komasaki (1985)] and carcinostatic drugs [Tsutsui and Kato (1988)].

2.2 Carbon Nanotubes

Carbon based nanofillers can exhibit tremendous physical, mechanical and thermal properties [Dresselhaus et al. (1996); Ajayan (1999); Dresselhaus et al. (2001); Meyyappan (2005); Coleman et al. (2006)]. Fullerene, a closed cage, was discovered in 1985 and with this discovery the history of these carbon-based nanoparticles began. The fullerene C_{60} is also called buckyball named by R. Buchminster Fuller. He was the architect of the geodesic domes. In 1996 Richard E. Smalley, Robert F. Curl and Harold W. Kroto received the Nobel Prize in Chemistry for the discovery of C_{60} in 1985. The design of the C_{60} molecule is famous since Leonardo da Vinci. In 1509 the mathematician Luca Pacioli published the regular truncated icosahedron in his book

“De Divina Proportione” but the design was made by Leonardo da Vinci. In biology the icosahedral symmetry can be found in viruses as well [Dresselhaus et al. (1996)].

Multi-wall Carbon nanotubes (MWCNT) were discovered by Iijima in 1991 [Iijima (1991)]. Carbon nanotubes are graphene sheets, which are rolled into a cylinder with a diameter of some nanometers [Ajayan (1999); Dresselhaus et al. (2001); Ganguly et al. (2008)]. In 1993 Iijima and Ichihashi (1993) and Bethune et al. (1993) discovered the single wall carbon nanotubes (SWCNT).

The latest discovered carbon based nanoparticle is graphene, which is a monolayer of graphite. Andre Geim and Konstantin Novoselov received the Nobel Prize in Physics for groundbreaking experiments with the two-dimensional material graphene in 2010.

In Fig. 2.1 the timeline of the research interest of different carbon based nanofillers are illustrated. It can be seen the interest especially for carbon nanotubes increased rapidly the last years. In Fig. 2.2 the structure of C_{60}, CNT and graphene can be seen. The huge variety of carbon materials can be classified in graphite materials (natural graphite), graphene (single 2D layer of graphite), graphite whiskers (scrolls of an atomic layer of graphite), carbon fibers, glassy carbon (graphite-like ribbons or microfibrils), carbon blacks, carbon coated carbide particles, porous carbon (carbon aerogels), liquid carbon, graphite intercalation compounds to name but a few [Dresselhaus et al. (1996)].

CNTs are a sheet of graphene, which is rolled into the form of a tube. The graphene is formed as a two-dimensional sheet of carbon atoms arranged in a hexagonal array. So the atomic structure of CNT is similar to that of graphite. The C-atoms bond to three neighbor atoms (sp2-hybridization) and form a regular hexagon [Dresselhaus et al. (1996)]. The end of the cylinder can be closed by two caps and each cap is a hemi-fullerene. The properties of the CNTs depend on the arrangement of the graphene sheets, the diameter, the length of the cylinder and the morphology [Thostenson et al. (2001)].

Due to the various possibilities to roll the graphene into a tube several different CNT types can be generated. In Fig. 2.3 it can be observed that the C-atoms for CNT formation can be described with a coordinate system. The chiral vector OA is defined on the honeycomb lattice of carbon atoms by unit vector a1 and a2 and the chiral

angle θ with respect to the zigzag axis. This graph (see Fig. 2.3) is constructed for (n,m)=(4,2) [Dresselhaus et al. (1996); Bharat (2010)].

In Fig. 2.4 the possible choices of n and m are explained. Below each pair of integers (n, m) is listed the number of distinct gaps that can be joined continuously to the carbon nanotube denoted by (n, m) [Dresselhaus et al. (1996); Saito et al. (1992)]. The red solid points represent metallic nanotube and the black open circle shows semiconductor CNTs.

The condition for the metallic nanotube is: n – m = 3r (r= 0,1,2, …) and for semiconductor n – m ǂ 3r (r= 0,1,2, …)

Armchair structure has n=m integers with an angle of about 30°. For the zigzag structure n=m=0 has to be formed. With all other roll directions a chiral structure can be designed, which can be seen in Fig. 2.5 [Dresselhaus et al. (1996); Saito et al. (1992)].

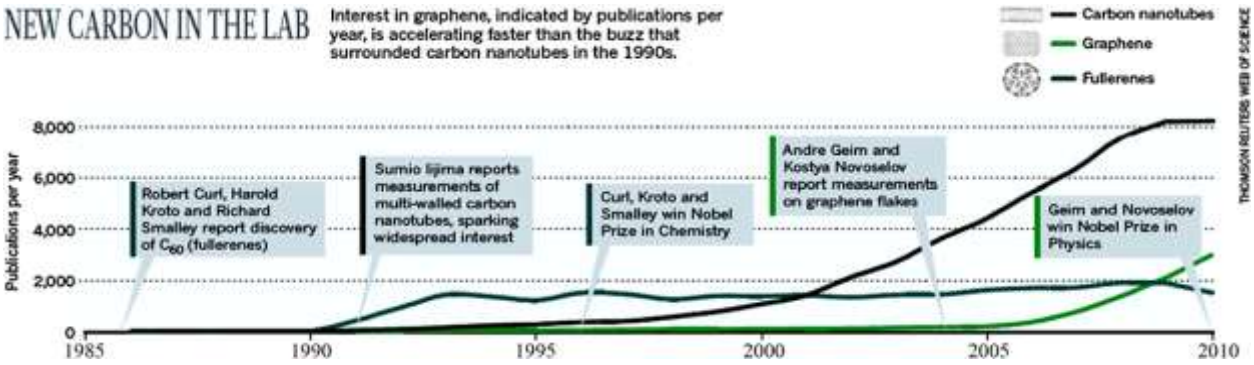

Fig. 2.1 Timeline of the carbon based nanoparticles' research interest [Noorden (2011)]

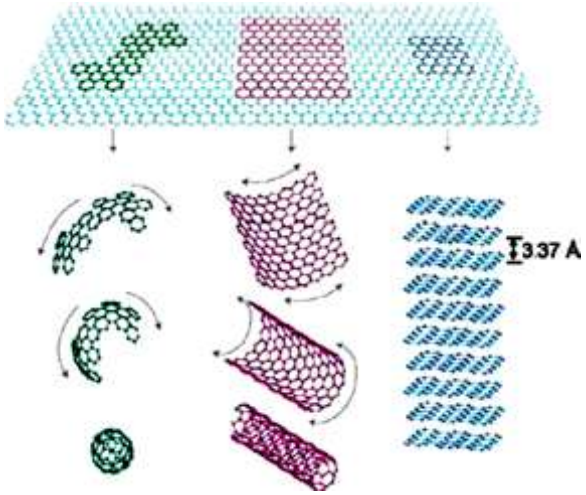

Fig. 2.2 Structures of C_{60} (left), CNT (middle) and graphene (right) [Geim and Novoselov (2007)]

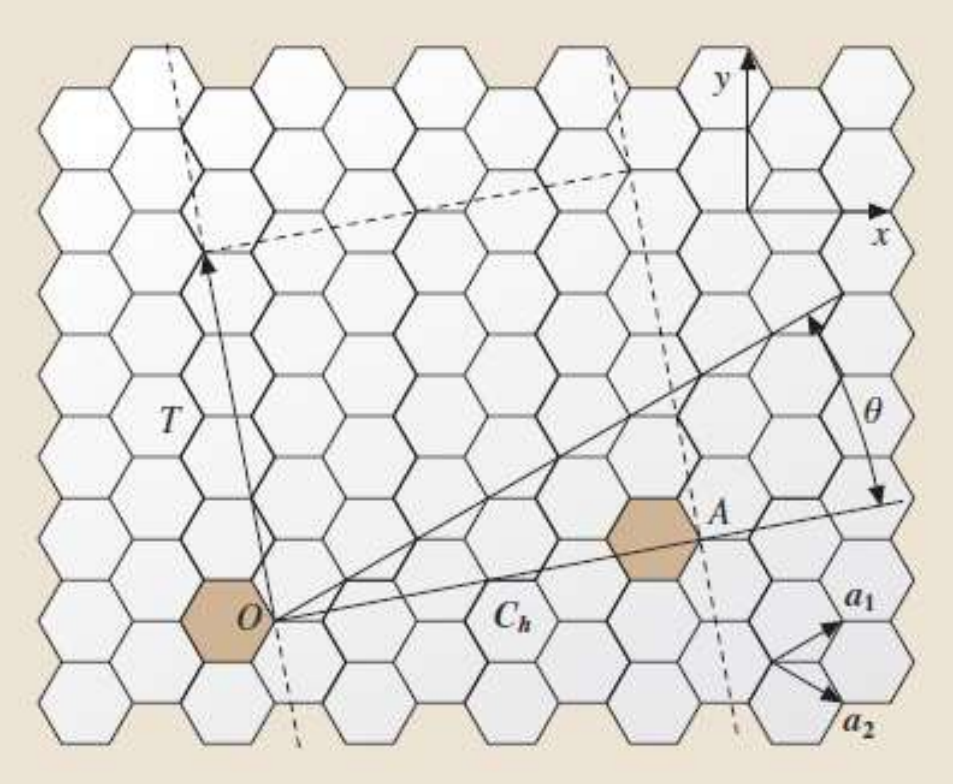

Fig. 2.3 Graphene sheet for the formation of CNTs [Dresselhaus et al. (1996); Bharat (2010)]

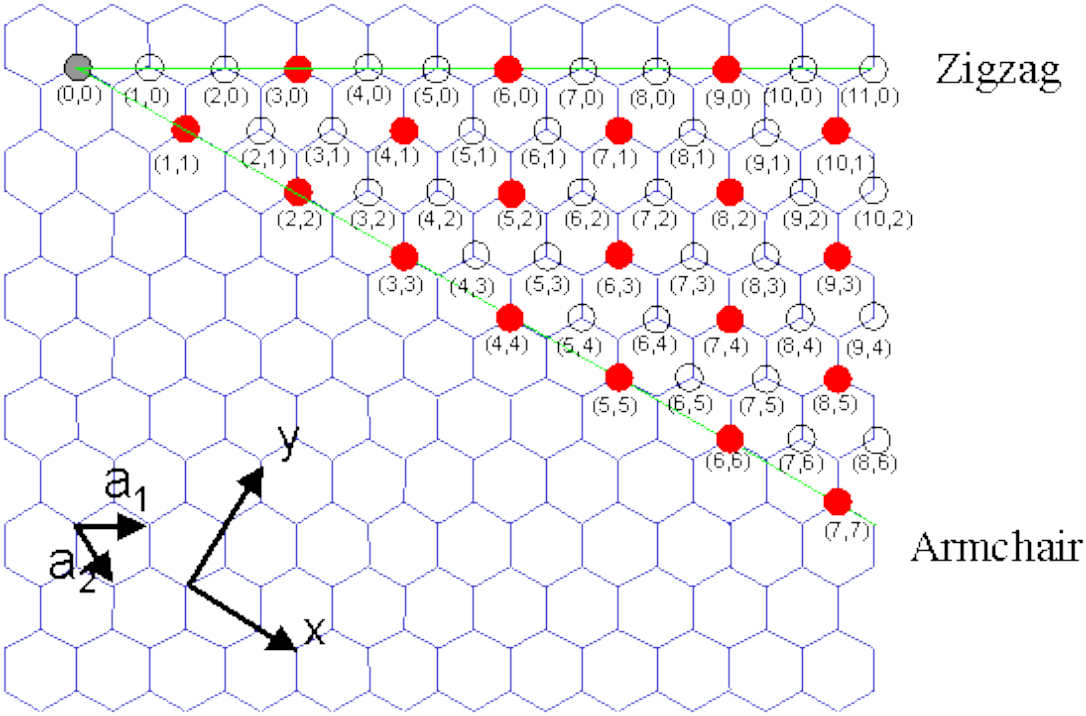

Fig. 2.4 Zigzag and armchair structure of CNT [Dresselhaus et al. (1996); Saito et al. (1992)]

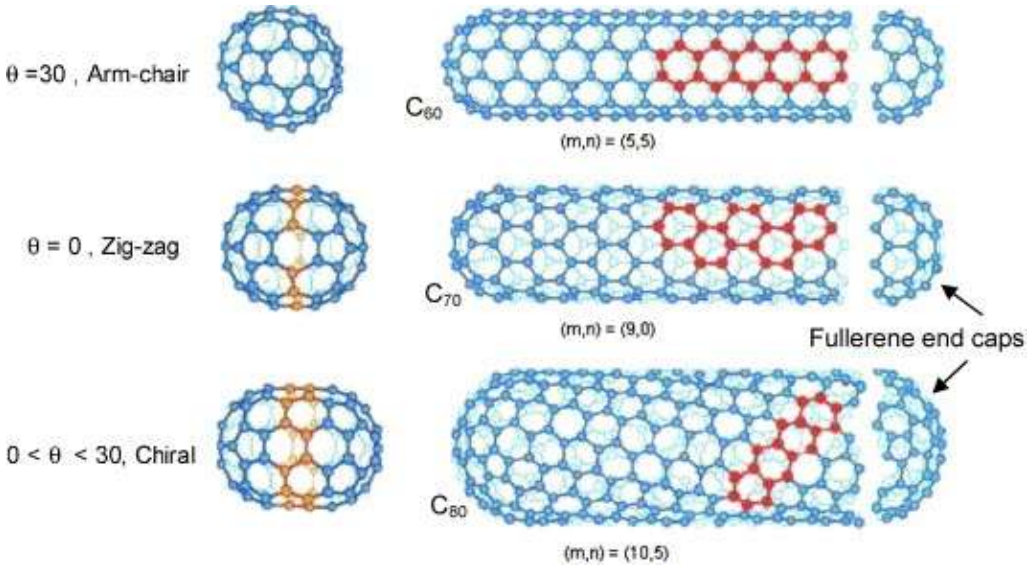

Fig. 2.5 Different structures of CNT with different possibilities of endings [Dresselhaus et al. (1996); Saito et al. (1992)]

Due to the different character (e.g. metal or semiconductor) of the different types of CNTs, the structure plays a great role. CNTs can be also classified by the number of walls: Single wall carbon nanotubes (SWCNT), double wall carbon nanotubes (DWCNT) and multi wall carbon nanotubes (MWCNT).

Other important factors of CNT are chirality, diameter and caps. These different characteristics lead to difference in mechanical and electrical behavior [Greßler et al. (2011); Monner et al. (2003); Krueger (2010)]. SWCNT show improved electrical properties and therefore preferred by the electronics industry due to their less liability to lattice defects. The explanation for the electrical conductivities is the molecular structure and the resulting band structure respectively different band gaps. By the way at very low temperatures several CNT can be superconductive [Brand et al. (2009)].

The advantage of DWCNT is the special chemical properties compared to SWCNT. While the chemical functionalization of DWCNT only takes place in the outer layer (contrast to SWCNT), the inner tube remains intact, which leads to good mechanical properties and retention of electronic properties [Ajayan (1999); Dresselhaus et al. (2001); Robertson (2004)].

MWCNT, which have a lower tensile strength and modulus than SWCNT, can be divided into various structures. The Russian doll structure consists of several concentric tubes, which are stacked into each other. The single tubes can be moved

apart like a telescope without friction. The parchment structure is similar to a convolved newspaper. To achieve this structure a single layer of graphite is curled up around itself [Greßler et al. (2011); Monner et al. (2003); Krueger (2010)].

CNT have an increased chemical reactivity because of the curvature of the surface and the deviation of planarity of sp2-hybridization. This effect is more expressed on the caps of CNT. Therefore the nanotubes can be easily covalent chemical modified, which is used to realize different solubility of CNT in different solutions [Brand et al. (2009)].

The multiplicity of CNT structures and properties can be compared with the huge amount of production techniques for CNT. SWCNT are produced by evaporation on a lanthanum particle, laser ablation, chemical vapor deposition (CVD), catalytic decomposition of C_{60} or growth by CVD on a catalytically patterned porous silicon substrate [Roy, Sengupta and Bhowmick (2012)].

MWCNT can be synthesized by non-catalytic and catalytic methods. The non-catalytic methods arc evaporation technique (similar to C_{60} synthesis), condensation of carbon vapor in the absence of an electric field, oven laser vaporization (similar to C_{60} synthesis), pyrolytic methods and electrochemical synthesis. The catalytic methods are CO disproportionation reaction and chemical vapor deposition. The most common used method is CVD with the disadvantage of highly entangled and agglomerated CNT [Sochor et al. (2012), Roy, Sengupta and Bhowmick (2012)]. But the properties of MWCNT are also affected by the properties of CNT and the polymer (e.g. melt viscosity) and not only by processing [Sochor et al. (2012)].

The CVD method has the greatest potential due to the high quantity production but with higher defect density. Carbon arc discharge and pulsed laser ablation are favorable for high purity CNT of defined structure. Arc evaporation produces also other nanoparticles and graphitic debris beside CNT [Roy, Sengupta and Bhowmick (2012)].

2.3 Sorbitol – POSS interactions

This research work is based on two PhD theses [Lee (2009); Roy (2011)], which were done in Dr. Jana's research group at the University of Akron (Department Polymer Engineering) and dealt with the sorbitol-POSS interactions in the polymer

matrix polypropylene. For a better understanding of the low liquid complex, formed by DBS and POSS, the main results are summarized in this section.

The DBS forms fibrillar network [Kristiansen et al. (2003); Thierry et al. (1992)] and POSS molecules self-assemble upon cooling in PP compounds [Capaldi et al. (2005)]. The formation of the fibrillar network is heavily dependent on the sorbitol concentration in PP. At higher concentration this network can be formed more easily. Less than 1 wt% amount of filler, DBS can act as an efficient nucleating agent. From 5 wt% DBS concentration the solubility is limited in PP and a separate phase is formed [Lee (2009)].

The fibrillar network is formed due to the self-assembly promoted by hydrogen bonding between DBS molecules [Kristiansen et al. (2003); Shepar et al. (1997)]. The beginning of gelation can be observed in rheological measurements. The loss tangent becomes independent of oscillatory shear frequency [Dumitras and Friedrich (2004); Fahrlander et al. (2000); Mercurio and Spontak (2001); Kuehne and Friedrich (2009)]. The start temperature of gel formation varies with the DBS filler content; at about 170°C with 0.5 wt% DBS (no detectable birefringent fibrillar crystals) and at about 190°C with 0.7 wt% DBS (endless fibrillar structure) [Lee (2009); Perilla et al. (2010)].

Lee (2009) also investigated the influence of different types of POSS (tri-silanol-phenyl-POSS and octa-isobutyl-POSS) on the DBS-POSS interactions. He found out that the hydrogen bonding between DBS and POSS was only possible with tri-silanol-phenyl-POSS due to the hydroxyl groups in the molecules of these compounds. Under the presence of tri-silanol-phenyl-POSS the fibrillar network of DBS is not formed easily. This is attributed to stronger interactions between this type of POSS and DBS than DBS-DBS interaction.

DBS fibrillation occurs as a result of complex interactions between DBS molecules and interactions between aromatic groups. So these interactions and hence the formation of the low liquid complex are influenced by the active functional groups of POSS. Tri-silanol-phenyl-POSS can interact with DBS via hydrogen bonds and via phenyl groups, while with octa-isobutyl-POSS it was not possible to form hydrogen bonds with DBS. This type of POSS consolidated the gel and increased the elasticity [Lee (2009); Perilla et al. (2010)].

At 10 wt% tri-silanol-phenyl-POSS this nanofiller cannot produce self-assembled structure in PP by itself, which could be seen in a reduction of the complex viscosity under the values of PP. With 0.7 wt% DBS and 0.5 wt% tri-silanol-phenyl-POSS the fibrillar network can be formed very easily. With 0.3 wt% DBS and 0.5 wt% tri-silanol-phenyl-POSS the fibrillation in the compound was subdued [Lee (2009)]. So the synergistic effect of these fillers is influenced by the ratio of the fillers.

The infrared (IR) spectroscopy results showed that DBS did not show any condensation reaction while tri-silanol-phenyl-POSS showed such reactions. Two different possibilities for condensation reactions can take place: between DBS and tri-silanol-phenyl-POSS and between tri-silanol-phenyl-POSS [Lee (2009)].

The molten nanocomposites filled with DBS and tri-silanol-phenyl-POSS solidified fast in the presence of the nucleating agent and thus providing higher melt strength. He proposed that bottom-up self-assembly of POSS from an initial dispersion of small POSS molecules generates POSS nanoparticles by shear-induced self-assembly process (see Fig. 2.6) [Lee (2009); Perilla et al. (2010)].

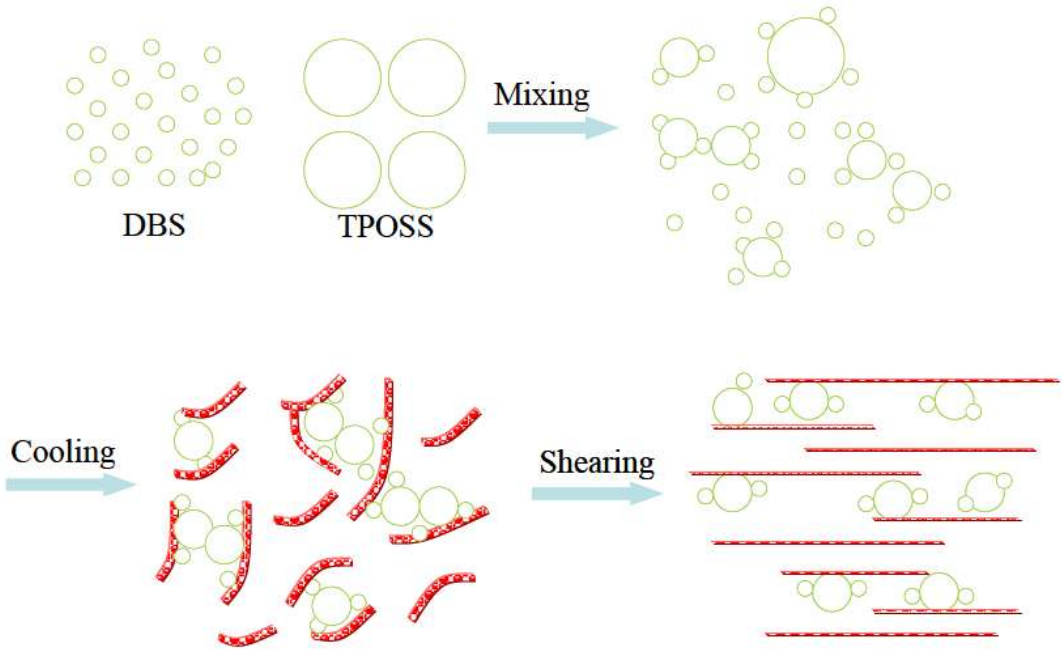

Fig. 2.6 Hypothesized mechanism for functioning of ph-TPOSS nanoparticles assisted by DBS fibrillar networks formed during mixing and shearing under in-situ observation. Lines with dot represent the self-organized networks of DBS molecules. [Lee (2009)]

Roy et al. (2011) found out that a minimum of 2 wt% tetra-silanol-phenyl-POSS or 5 wt% of tri-silanol-phenyl-POSS is needed for complete suppression of fibrillation of 1 wt% DBS. Because of the additional silanol group per molecule in tetra-silanol-phenyl-POSS a muss less amount of filler is needed than with tri-silanol-phenyl-POSS for the subduing the DBS fibrillation. The tri-silanol-cyclo-pentyl-POSS showed much less interactions with DBS that could be observed as an upturn of viscosity. Although tri-silanol-phenyl-POSS and tri-silanol-cyclo-pentyl-POSS have the same number of silanol groups per molecule, DBS fibrillation was not completely subdued even in the presence of 10 wt% tri-silanol-cyclo-pentyl-POSS.

Roy et al. (2011) indicates that hydrogen-bonding interactions are not the only possible interactions in the nanocomposites. He also observed additional π-π stacking interactions derived from the phenyl functionalities, which enhance the stability of the low-viscosity liquid complex.

Therefore the combination of 5 wt% tri-silanol-phenyl-POSS with 1 wt% DBS was used in this research work. These synergistic combinations transform the mixture of crystalline POSS and DBS into transparent low-viscosity complex upon heating at 200° C. It generates a liquid which is amenable to deformation and breakup into small droplets in shear and extensional flows. This liquid upon solidification generates hard particles or potential reinforcement of the polymer [Roy et al. (2011)].

Roy et al. (2012) also investigated the influence of fiber spinning process on the low-viscosity liquid complex. Due to the complex the complex viscosity is reduced significantly. Therefore it was possible to spin fibers with a much smaller diameter than achievable only with the neat PP. Upon cooling the melt spun fiber the molecular adducts turned into cylindrical solid nanoparticles. He also observed a large enhancement in tensile properties of the melt spun fibers with high draw down ration due to the polymer chain orientation and not due the presence of POSS [Roy (2012)].

In his third paper Roy (b) (2012) analyzed different types of POSS. He observed that POSS molecules with no phenyl side groups and POSS molecules with phenyl side groups but without silanol groups cannot subdue DBS fibrillation in iPP. The presence of silanol and phenyl groups is beneficial for DBS/POSS interactions leading to self-assembly. Non-phenyl and non-silanol POSS showed phase

separations and aggregated crystals. The silanol-POSS with isobutyl side groups / DBS compound formed a marginal complex and with iso-POSS the DBS could not form any complex [Roy (b), 2012].

3 EXPERIMENTALS

In this section the various used materials, processing steps and characterization methods are described. In the case of necessary reproducing of the experimental work a picture is provided for each device.

3.1 Materials

3.1.1 Polypropylene

The isotactic polypropylene P4G2Z-159 (iPP) was supplied by Flint Hill Resources (Wichita, Kansas, US) with MFR 1.95 g/ 10 min and crystalline melting temperature (T_M) of 165°C. This iPP does not contain any nucleating agent and it is recommended for extrusion (BOPP films). In this research work this PP type was used as polymer matrix. In Table 3.1 the PP's properties are shown according to the material data sheet.

Table 3.1: Material data of iPP P4G2Z-159 according to the material data sheet

Properties	Values (ASTM)
Density	0.9 g/m^3 (D 1505)
Melt Flow Rate	1.95 g / 10 min (D 1238)
Tensile – yield strength	37 MPa (D 638)
Tensile – yield elongation	9 % (D 638)
Flexural Modulus – 1 % secant	1483 MPa (D 790)
Flexural Modulus - Tangent	NA
Deflection Temperature @ 0.455 MPa	92°C (D 648)
Rockwell Hardness	105 R (D 785)
Notched Izod @ 23ºC	30 J/m (D 256)
Gardner Impact @ 23ºC	13 J (D 5420)

3.1.2 Sorbitol di-benzyliden-sorbitol

The sorbitol di-benzyliden-sorbitol (DBS) was used for this research work. DBS Millad 3905 (M_w = 358.4 g/mol, T_M = 225 °C) was obtained from Milliken Chemicals (Spartanburg, SC, US) in the form of white powder and it has two free –OH groups with phenyl side rings. The chemical structure can be seen in Fig. 3.1.

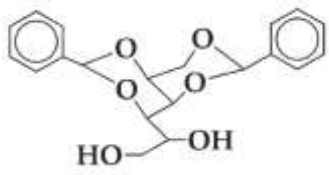

Fig. 3.1 Chemical structure of DBS

3.1.3 Tri-silanol phenyl-polyhedral oligomeric silsesquioxane

The tri-silanol phenyl-polyhedral oligomeric silsesquioxane (tri-POSS; M_w = 930.07 g/mol and T_M = 230 °C) were supplied by Hybrid Plastics (Hattiesburg, MS, US). Tri-POSS has three silanol groups (see Fig. 3.2). This filler was also used in the form of a white powder.

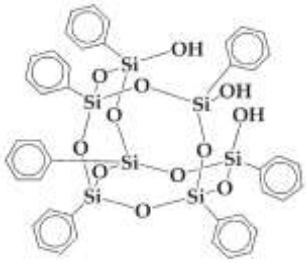

Fig. 3.2 Chemical structure of tri-POSS

3.1.4 Carbon Nanotubes

For this research topic unmodified MWCNTs Graphitstrength® C100, which were supplied by Arkema, King of Prussia, PA, USA, were used with a diameter of 10 to 15 nm and a length of 0.1 to 10 µm (see Fig. 3.3). The average walls of the MWCNTS are from 5 to 15.

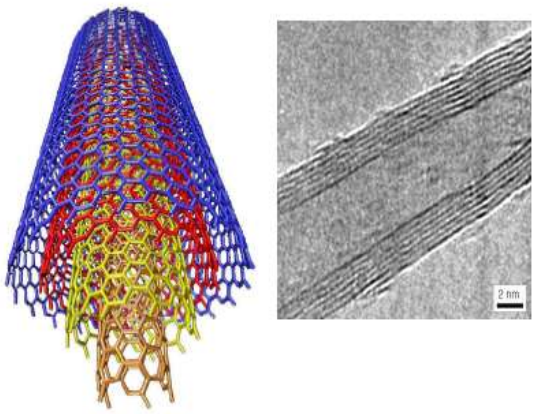

Fig. 3.3 Images of multi wall carbon nanotubes [Bordere et al. (2005)]

3.1.5 Nanosilicon

The nanosilicon was used as unmodified and modified filler. According to confidentiality the modification of this filler is not described in this report.

3.1.6 Synthetic amorphous precipitated silica

The used silica was used in form of a white powder and was supplied by Evonik Degussa Corporation, Parsippany, NJ, US. Silica was incorporated in the polymer matrix without modification.

3.2 Processing of polymer nanocomposites

The main objective of this section is the description of the processing machines and parameters, which were used for this research work. The compounds were produced in an internal mixer Brabender Plasticorder Type PL2000 (Duisburg, Germany). In Fig. 3.4 the Brabender is shown.

Fig. 3.4 Laboratory kneader Brabender Plasticorder Type PL2000

The processing temperature was 185°C and the screw rotation speed was varied between 30 rpm and 80 rpm. After melting the iPP, the additives DBS and POSS were added in the mixing chamber. After ten minutes kneading, the other fillers were incorporated so that the low viscosity liquid complex could be formed prior to that. Before mixing all additives were dried at 80°C for 24 h. The single steps of processing are described in Fig. 3.5.

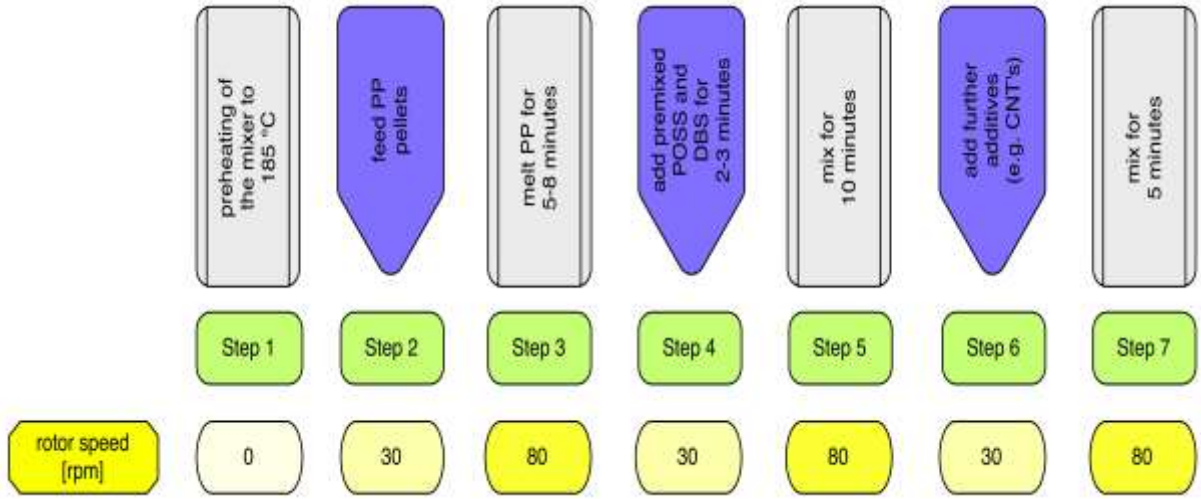

Fig. 3.5 Single processing steps for the production of PP nanocomposites

After processing with the laboratory kneader the compounds were dried and ground into small pellets for further processing and investigations. The grinder of the company weima (Fort Mill, SC, USA) can be seen in Fig. 3.6.

Fig. 3.6 Grinder for pelletizing

For the rheological properties the compounds were molded for 5 min at 200°C in a vacuum compression mold of company Technical Machine Products Inc. TMP (Cleveland, OH, USA), which can be seen in Fig. 3.7. Due to the missing cooling system of this machine, the compressed materials were cooled in another hydraulic compression mold, which is not depicted.

Fig. 3.7 Compression molding machine

3.3 Fiber Spinning of PP nanocomposites

The fibers were spun with the help of capillary rheometer ROSAND RH7 (Malvern Instruments Ltd., Malvern, UK) and a home-made take up device (see Fig. 3.8 and 3.9). The length to diameter ratio was 32:2 and the plunger speed $v_{plunger}$ was varied between 0.2 and 2 mm/min. The take-up velocity was between 10 rpm and 120 rpm at a melt temperature of 200°C and cooled down to room temperature during rolling-up. The draw down ratio (DDR) of the melt spun fibers was calculated as in eq. 3.1 with the velocity of fiber take-up (v_{fiber}), the velocity of melt (v_{melt}) at the die, the diameter of the bobbin (D_{roll} 85 mm), the winding speed (Ω), the radius of barrel (R_{barrel} 15 mm) and the radius of the die R_{die}. The diameters of the fibers were measured with an optical microscope (magnification of 100x) Olympus BX60 (Olmypus, Center Valley, PA, USA) and a camera Canon EOS Rebel T2i (Canon, Lake Success, NY, USA), which can be seen in Fig. 3.9. The optical microscopy images were aligned with the software ImageJ.

$$\mathrm{DDR} = \frac{v_{fiber}}{v_{melt}} = \left(\frac{D_{die}}{D_{fiber}}\right)^2 = \left(\frac{\pi\, D_{roll}\, \Omega}{R_{barrel}/R_{die}}\right) v_{plunger} \quad \ldots (1)$$

Fig. 3.8 Capillary rheometer (left), home-made take up device with bobbin (right)

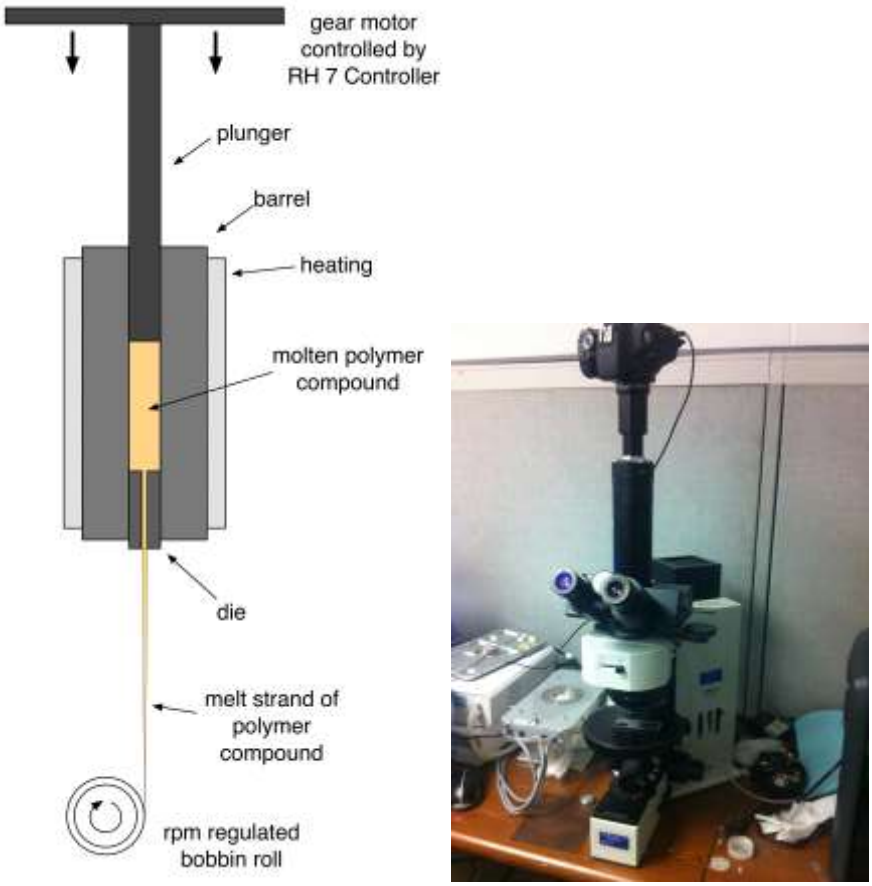

Fig. 3.9 Schematics of the fiber spinning set-up (left), optical microscope (right)

3.4 Characterization methods

3.4.1 Rotational viscometer

The rheological properties were investigated by using a rotational rheometer “an advanced rheometric expansion system” (ARES) of 1st generation from TA Instruments (New Castle, DE, US) with parallel plate set-up and without a liquid nitrogen atmosphere (see Fig. 3.10). To ensure that the strain used is within the linear viscoelastic range, strain sweep tests were performed for each material. The strain was fixed with 2 %. The storage G’, the loss modulus G’’ and the complex viscosity η* were measured over a frequency range of 1 to 100 rad/s at 200 °C. The specimens had a diameter of 25 mm and a thickness of 2 mm. Two different test methods were applied for the characterization of the PP nanocomposites. First, the specimens were heated to 220 °C and kept for about 5 min to be sure that the specimen is molten. Then the complex viscosity was measured from 220 °C to 120 °C at a rate of 10 °C/min at a constant angular frequency of 10 rad/s. Second, the complex viscosities were determined by frequency sweep tests at 200 °C (viscosity range from 100 to 1 rad/s. The specimens were heated to 220 °C for about 5 min. The strain rate was kept small (2 %) to insure that the structure of the DBS was not significantly disturbed by the applied shear. The data were evaluated using the software TA Orchestra (TA Instruments, New Castle, DE, US).

Fig. 3.10 Rotational rheometer ARES (1st generation)

3.4.2 Tensile Testing

For characterization of the mechanical properties of the fibers an Instron tensile test (Model 5567) with a 5 N load cell was used (see Fig. 3.11). The tensile tests were performed with a crosshead speed of 50 mm/min and a gauge length of 26 mm at room temperature according to ASTM D3822. For the sample preparation single fibers were mounted on a preformed paper (see Fig. 3.11). For each material at least 10 specimens were tested.

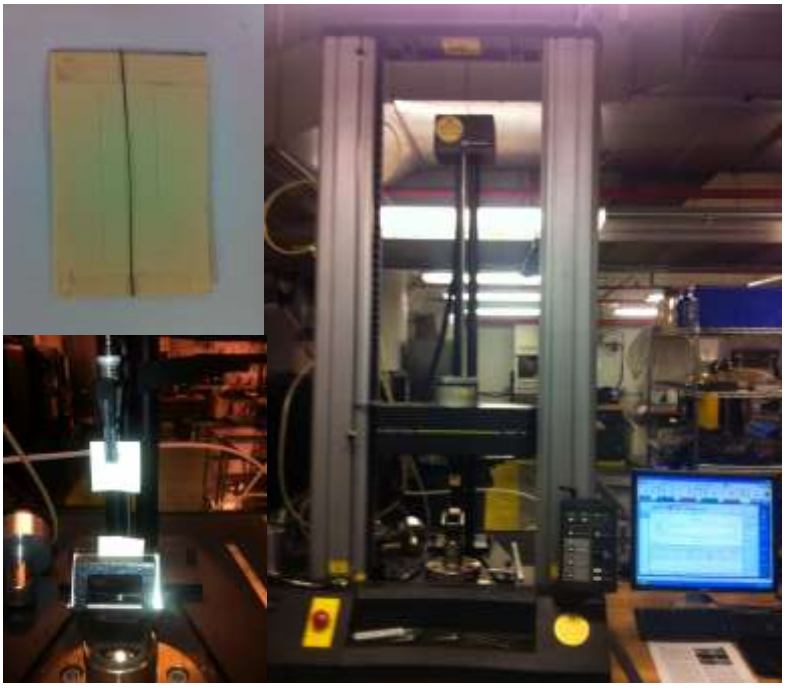

Fig. 3.11 Sample preparation method for fibers (left top), tensile testing set-up (left below and right)

3.4.3 Differential Scanning Calorimeter

The thermal analyses were carried out with a Differential Scanning Calorimeter (DSC) Q2000 (TA Instruments, New Castle, DE, USA) under nitrogen atmosphere (see Fig. 3.12). The melt-mixed compounds and fibers were heated from 30 to 200 °C (heat rate 10 °C/min), kept at 200 °C for 5 min and cooled to 30 °C (cooling rate 10 °C/min). For heating and cooling (under quiescent conditions) scans the crystallinities were calculated as in eq. 2 with the enthalpy of nanocomposite (ΔH_m) to the enthalpy of fusion of 100 % crystalline iPP (ΔH_0 = 177 J/g) [Lee et al. (2004)].

$$\chi_c = \frac{\Delta H_m}{\Delta H_0} * 100\ \% \quad \ldots (2)$$

Fig. 3.12 DSC Q2000 (TA Instruments, New Castle, DE, USA)

3.4.4 Scanning electron microscopy

The characterization of the fibers' morphology was carried out with the scanning electron microscopy (SEM) JEOL JSM 5310 (JEOL, Tokyo, Japan) at an operating voltage of 10 kV (see Fig. 3.13). The fibers were fixed in epoxy resin and fractured after soaking in liquid nitrogen. The surface of the sample was sputter-coated with 1.5 min using Sputter coater ISI 5400 under argon gas atmosphere.

Fig. 3.13 SEM JEOL JSM 5310 (JEOL, Tokyo, Japan)

3.4.5 Transmission electron microscope

The morphology of the DBS/POSS/CNT solution were characterized with a transmission electron microscope (TEM) JEOL JEM 1200 XII (JEOL, Tokyo, Japan), which is depicted in Fig. 3.14. The fillers were solved in tetrahydrofuran and drop casted on a copper TEM grip.

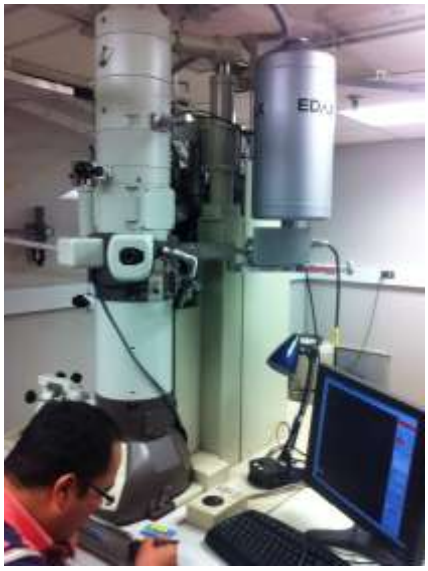

Fig. 3.14 TEM JEOL JEM 1200 XII (JEOL, Tokyo, Japan)

3.4.6 Wide angle X-ray diffraction

The orientation factors of the fibers were analyzed using a Bruker AXS D8 Discover (Bruker AXS Inc., Madison, WI, USA) wide angle X-ray diffraction (WAXD) equipment with 40 kV and 40 mA with a beam monochromatized to CuKα radiation wavelength (λ) of 1.54 Angstroms (see Fig. 3.15). The fiber samples were mounted around a metal frame and measured for 3 min. For comparison the total diameter of the fiber bundle in each measurement was kept constant.

The orientation factors were calculated using Herman-Stein orientation factor of the crystalline regions assuming rotational symmetry using eq. 3-5, where $f_{a,z}$, $f_{b,z}$ and $f_{c,z}$ are the orientation factors for the different crystallographic axis and the $\cos^2 x_{a,z}$, $\cos^2 x_{b,z}$ and $\cos^2 x_{c,z}$ are the mean square cosine of orientation angle of the crystallographic axis [Stein (1958); Alexander (1969); Wilchinsky (1960); Nadella et al. (1977); Afshari et al. (2005)]. As in eq. 6 can be seen two orientations are enough to determine the orientation function. The strongest peaks for iPP in the diffractogram are the (110) and (040) planes and Wilchinsky developed a calculation of the mean

square cosine from the different diffraction planes of the I(X, Φ) function [Wilchinsky (1959); Wilchinsky (1963)], which can be observed in eq. 7 and 8. The equation 9 explains the relationship for the average cosine squared of the angle between the fiber axis and the c-axis [Nadella et al. (1977); Arvidson et al. (2010)].

The relative crystallinity x_c of the fibers was calculated according to Hermans and Weidingeer equation (see eq. 10), where A_c and A_a are the total crystalline and amorphous areas of the measured diffractogram [Hermans and Weidingeer (1961)]. In Fig. 3.16 a representative diffractogram for iPP can be seen, where the crystalline and amorphous areas are depicted.

$$f_{a,z} = \frac{3\cos^2\chi_{a,z} - 1}{2} \quad \dots (3)$$

$$f_{b,z} = \frac{3\cos^2\chi_{b,z} - 1}{2} \quad \dots (4)$$

$$f_{c,z} = \frac{3\cos^2\chi_{c,z} - 1}{2} \quad \dots (5)$$

$$f_{a,z} + f_{b,z} + f_{c,z} = 0 \quad \dots (6)$$

$$\cos^2\chi_{b,z} = \cos^2\chi_{040,z} = \frac{\sum_{\chi=0}^{90} I(\chi)_{040} \sin\chi\cos^2\chi}{\sum_{\chi=0}^{90} I(\chi)_{040} \sin\chi} \quad \dots (7)$$

$$\cos^2\chi_{110,z} = \frac{\sum_{\chi=0}^{90} I(\chi)_{110} \sin\chi\cos^2\chi}{\sum_{\chi=0}^{90} I(\chi)_{040} \sin\chi} \quad \dots (8)$$

$$\langle\cos^2\chi_{c,z}\rangle = 1 - 1.099\,\langle\cos^2\chi_{110,z}\rangle - 0.901\,\langle\cos^2\chi_{040,z}\rangle \quad \dots (9)$$

$$x_c = \frac{A_c}{A_c + A_a} \quad \dots (10)$$

Fig. 3.15 WAXD Bruker AXS D8 Discover (Bruker AXS Inc., Madison, WI, USA)

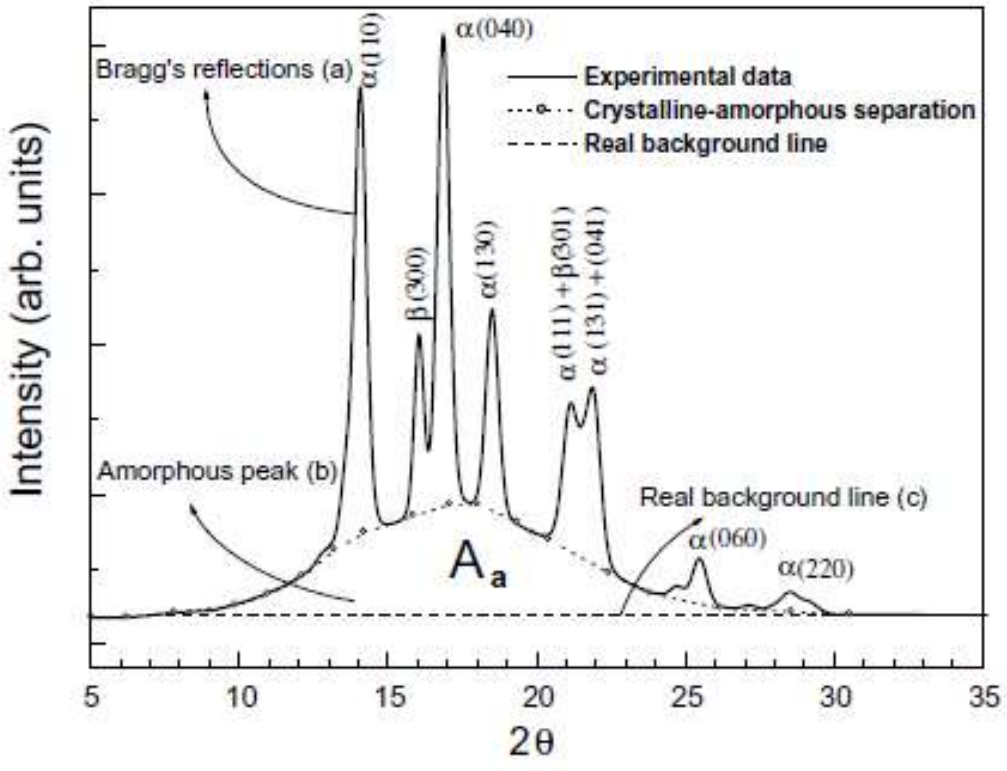

Fig. 3.16 Representative WAXD diffractogram for iPP with crystalline and amorphous areas [Machado et al. (2005)]

3.4.7 Polarized optical microscope

The changes of morphology of the PP/DBS/POSS/CNT nanocomposites during cooling were determined by using a polarized optical microscope (POM). Thin layers of the melt mixed samples were attached between two glass slides and heated up to 240 °C with the help of a hot stage. During cooling several pictures were taken with Olympus BX60 (Olmypus, Center Valley, PA, USA) at highest possible magnification of 100 x.

3.4.8 X-ray photoelectron spectroscopy

With X-ray photoelectron spectroscopy (XPS) PHI 5000 VersaProbe II (Ulvac Inc., Kanagawa, Japan) the CNTs, in form as a powder, were characterized (see Fig. 3.17). XPS is a surface analysis method, which gives information about the chemical state and surface quantity.

Fig. 3.17 XPS PHI 5000 VersaProbe II (Ulvac Inc., Kanagawa, Japan)

4 RESULTS AND DISCUSSION

In this chapter the results of the different characterization methods are collected and discussed. Within the several analysis methods the influences of different nanofillers such as CNT on the low viscosity liquid complex of iPP/DBS/POSS/ compounds were investigated.

4.1 Influence of processing on formation of low viscosity liquid complex

The topic of this research project is based on two dissertations dealing with the interaction between DBS and POSS in iPP, which were supervised by Prof. Jana (Department Polymer Engineering – The University of Akron). They found out that the adequate ratio between DBS and POSS for iPP is 1:5 wt%. This ratio was used for the whole research project. The first step was to reproduce the iPP/DBS/POSS compound to have the same starting point. The rheological measurements were used as control because only the compounds with a formed low viscosity liquid complex show the significant reduction in the complex viscosity.

A very important factor for adequate rheological results is the right processing. First, the production of the iPP/DBS/POSS compound was done with a relative small laboratory kneader (material savings), with which no reduction in the complex viscosity was achieved. There was no change in the results with the variation of screw geometry or processing time. Therefore the iPP/DBS/POSS compounds were processed with the standard used Brabender (larger chamber volume) and due to the higher shearing forces than with the smaller Brabender a significant reduction in the complex viscosity was received, which can be seen in Fig. 4.1. Only with higher shearing the low viscosity liquid complex could be formed and therefore the larger Brabender was used for the whole research project.

Second, different processing techniques for the formation of the DBS/POSS complex were tested. The best result was achieved with the addition of the powder mixture during kneading. No complex was formed with the method of DBS/POSS premixing in the oven at 200°C (see Fig. 4.2). For this reason the iPP/DBS/POSS compounds were produced with the addition of the powder mixture during the kneading.

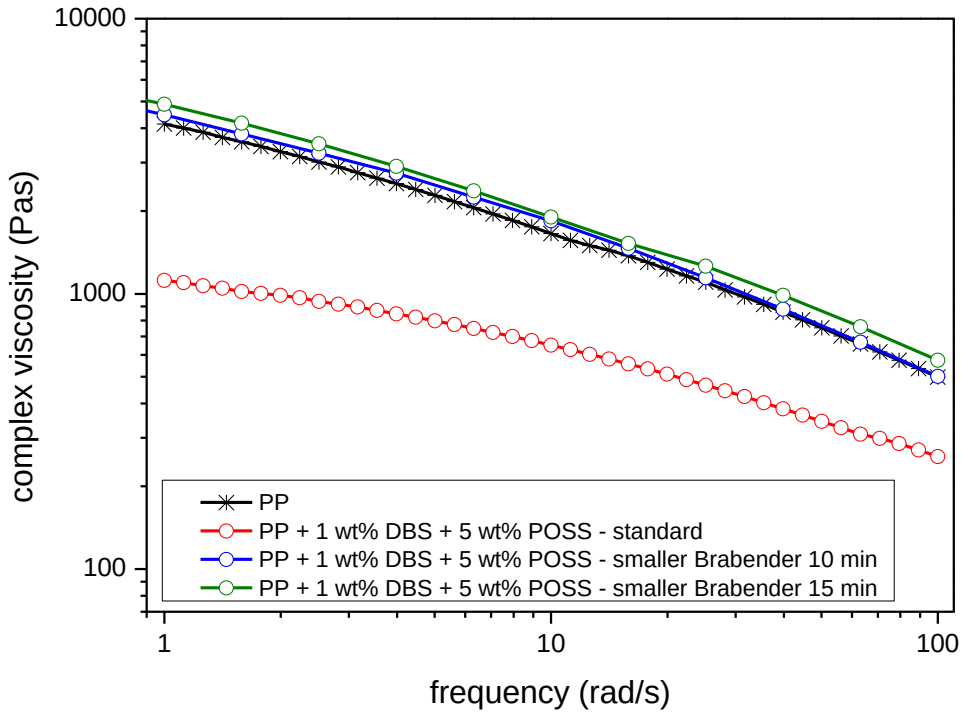

Fig. 4.1 Different processing methods for producing iPP/DBS/POSS compound

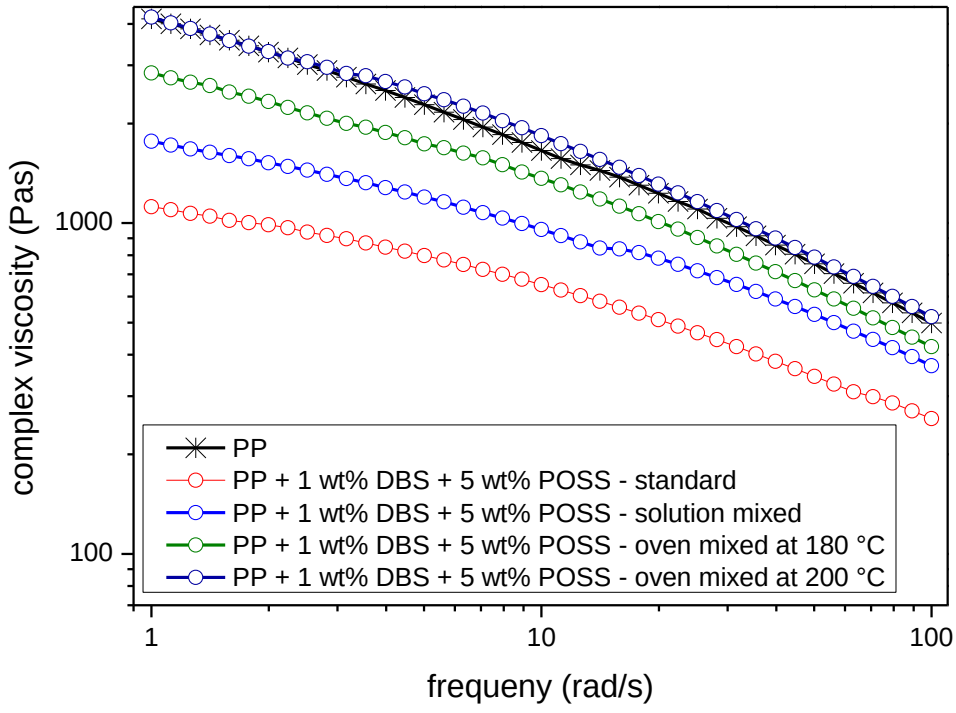

Fig. 4.2 Various methods for the formation of the low viscosity liquid complex

4.2 Rheological properties

Rheology is a very advantageous tool for the determination of molecular structure and the state of dispersion of nanofillers in a polymer matrix. Rheology is crucial to gain fundamental understanding of the processability, degree of polymer-filler interactions and structure-property relationships in polymer nanocomposites (PNC) [Ray (2006); Wagner and Reisinger (2003)].

In the first step the different methods for adding CNT to iPP were tested (see Fig. 4.3). It can be seen that only with the addition of CNT after forming the low viscosity liquid complex could achieve the reduction in viscosity. Adding CNT first and after 10 min mixing adding DBS and POSS leads to the formation of the fibrillar network of DBS, which can be identified by the shoulder at about 160 °C. When all nanofillers were put together and mixed together for about 10 minutes the complex viscosity look similar to the curve of the unfilled polymer.

In Fig. 4.4 the complex viscosities of iPP nanocomposites in dependency of the temperature are depicted. The sudden increase of the complex viscosities at lower temperature is because of the onset of iPP crystallization [Perilla et al. (2010)]. Roy et al. (2012) found out that the complex viscosity of iPP/DBS/POSS compounds decreases due to the formation of low viscosity liquid complex. The reduction of the complex viscosities at about 220° C, which can be only seen in the compounds with DBS, is due to the dispersion of the low viscosity liquid DBS in iPP [Roy et al. (2012); Balzano et al. (2008)]. It is also evident that the complex viscosity of iPP/DBS/tri-POSS compounds is significantly lower than that if iPP due to the low viscosity liquid complex of DBS and tri-POSS [Roy et al. (2011); Roy et al. (2012)].

The complex viscosity increases with the addition of CNT in iPP indicating the formation of an effective network of CNT [Ganß et al. (2008)]. The complex viscosity of PP/DBS/POSS compounds increases with the addition of CNT. Adding 2 wt% CNT the complex viscosity increases to the level of unfilled iPP. At the curves of complex viscosities for PP+1 wt%DBS+5 wt% POSS+1 wt% CNT and PP+1 wt%DBS+5 wt% POSS+2 wt% CNT a shoulder at about 150°C can be seen. The slight shoulder at about 160 °C is attributed to the development of a gel network by DBS, which can be normally observed in iPP/DBS compounds [Kristiansen et al. (2005); Kristiansen et al. (2003); Zhao and Schiraldi (2005)]. Similar phenomenon is

observed in shear viscosity data of compounds containing tri-POSS, DBS, and 1 wt% nSi; a shoulder at about 160 °C is attributed to fibrillation of DBS.

In contrast, the silica particles did not disturb the complex between DBs and tri-POSS; the complex viscosity of the compound of iPP, 1 wt% silica, DBS, and tri-POSS show viscosity similar to iPP melt; no separate shoulder attributed to DBS fibrillation is seen.

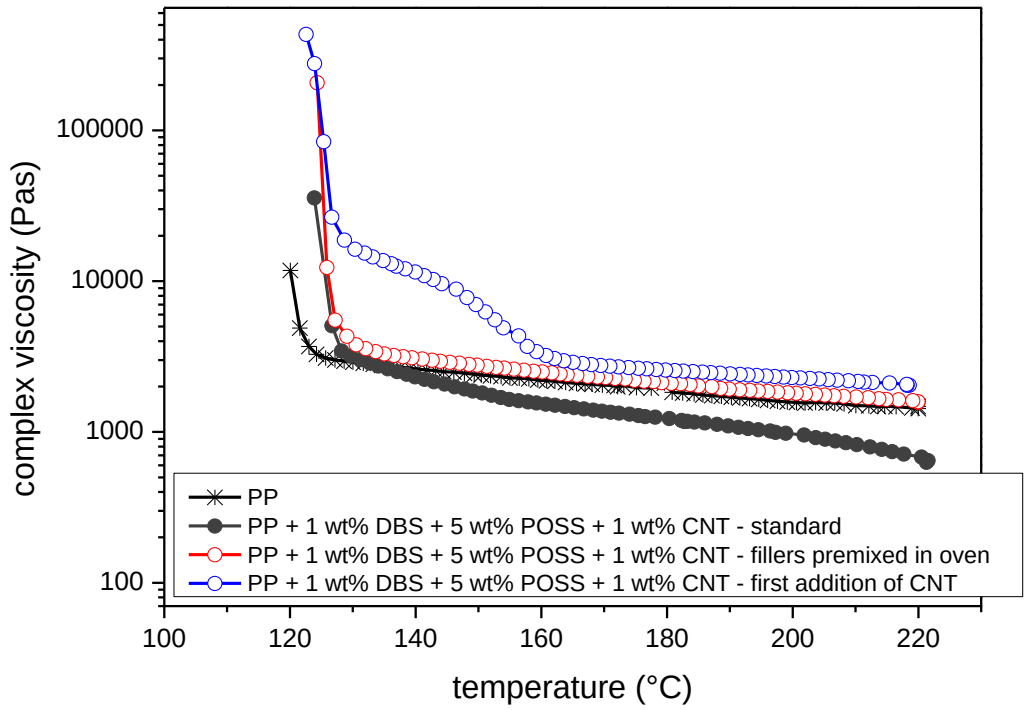

Fig. 4.3 Complex viscosity in dependency of the temperature for iPP/DBS/POSS/ 1 wt% CNT nanocomposites

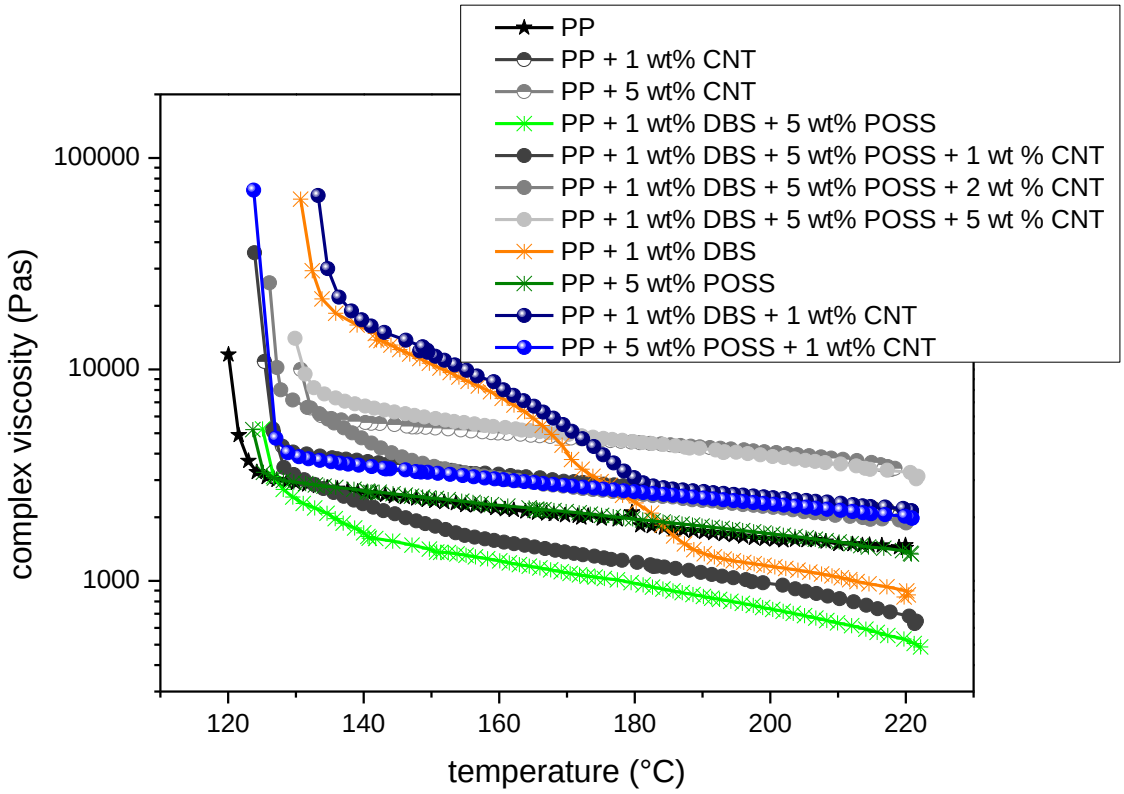

Fig. 4.4 Complex viscosity in dependency of the temperature for nanocomposites filled with CNT

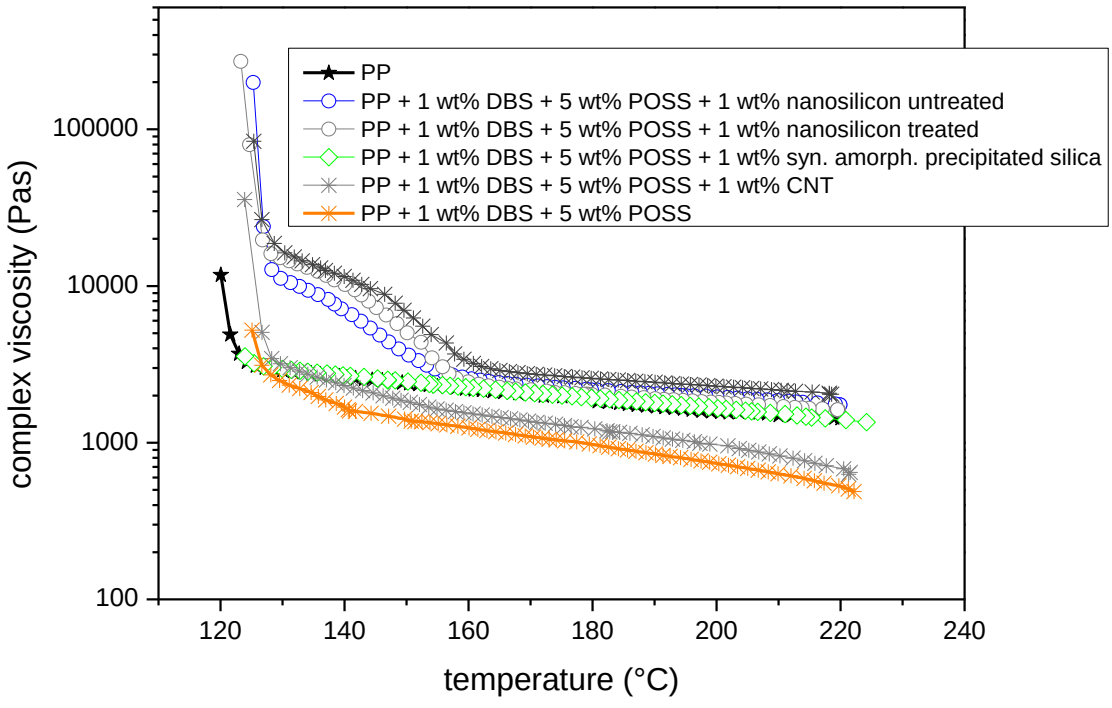

Fig. 4.5 Complex viscosity in dependency of the temperature for nanocomposites filled with CNT

4.3 Draw Down Ratio

During melt spinning of fibers the process can be controlled by different parameters such as the piston speed, die geometry and hereby resulting the draw down ratio (DDR). The DDR represents the elongation of the polymer strand after the die opening until solidification. For the characterization of PNC the DDR can give information about the deformation properties of the molten PNC and the influence of the nanofiller on the melt strength.

The maximum value of the draw down ratio (DDR) for each compound can be seen in Fig. 4.6. The compound iPP/DBS/tri-POSS shows the highest value of DDR. Recall that DBS and tri- POSS were present in this compound as a low viscosity liquid complex, which caused a reduction of the compound viscosity (see Fig. 4.4). The addition of CNT, nSi, and silica to the compounds caused a reduction of DDR, but such values are still higher than unfilled iPP. The highest DDR values for iPP/DBS/tri-POSS compounds containing CNT were at 2 wt% CNT content. The maximum value of the DDR for differently processed compounds and compounds containing silica, untreated nanosilicon and treated nanosilicon can be seen in Fig. 4.7. The premixing of DBS and POSS leads to a further decreased maximal DDR value, but remains still higher than unfilled PP. Supposedly the low viscosity liquid complex is not formed properly by this technique. The DDR of silica filled iPP/DBS/tri-POSS compound is on the same level as for CNT as filler. Untreated nanosilicon filled compound increases the maximum DDR above the values achieved by CNT filled compound. The treatment of nanosilicon improves the properties of the filler so a maximum DDR comparable to the values of unfilled iPP/DBS/tri-POSS compounds can be achieved. Presumably the surface treatment of the nanosilicon improves the mutual interaction between the filler and the iPP/DBS/tri-POSS compound and enhances thereby the fiber spinning properties.

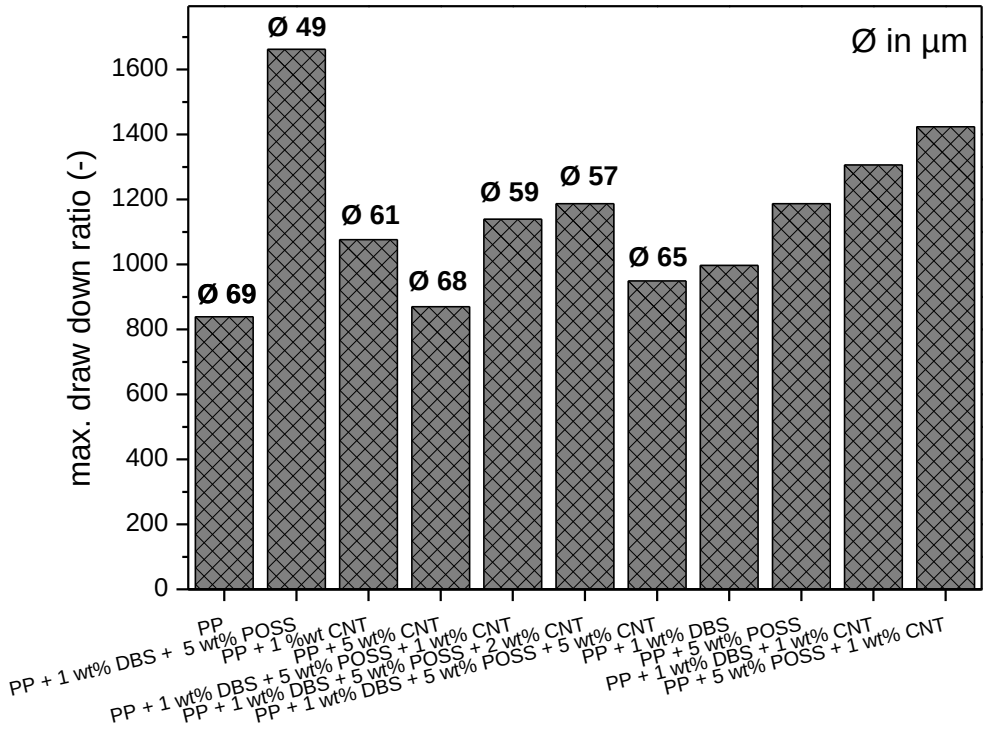

Fig. 4.6 Maximum draw down ratios of iPP/DBS/POSS nanocomposites filled with synergistic combinations of CNT

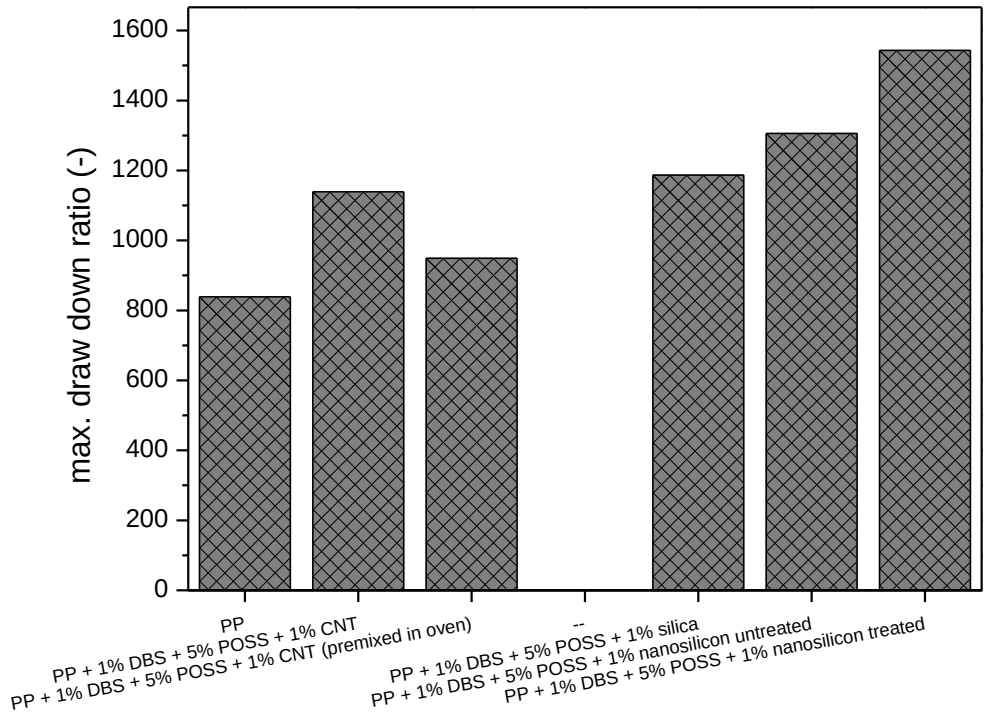

Fig. 4.7 Maximum draw down ratios of iPP/DBS/POSS nanocomposites filled with various nanofillers

4.4 Mechanical Properties

Mechanical properties like Young's modulus, elongation at break and stress at break deliver information about the basic properties of different materials and they allow a good comparison between them. Compounds containing silica and nanosilicon could not be tested regarding their mechanical properties due to the end of the research stay.

The Young's moduli of the produced compounds are depicted in Fig. 4.8, the strain at break values in Fig 4.9 and the elongation at break values in Fig. 4.10. The values of the fiber produced with maximum DDR are higher as those of the fibers produced with a DDR of 791, except for compounds containing only iPP/DBS/tri-POSS and 1 wt% CNT. iPP/DBS/tri-POSS nanocomposites show decreasing Young's moduli with increasing CNT content. None of the produced compounds could achieve strain at break values like unfilled iPP. Too high content of CNT and wrong production technique has a massive influence on the strain at break values. The elongation at break values shows rather uniform values for all iPP/DBS/tri-POSS compounds with and without CNT as filler, except for increased contents of CNT. For the mechanical results the different PP crystals phases can be responsible [Karger-Kocsis (1999)].

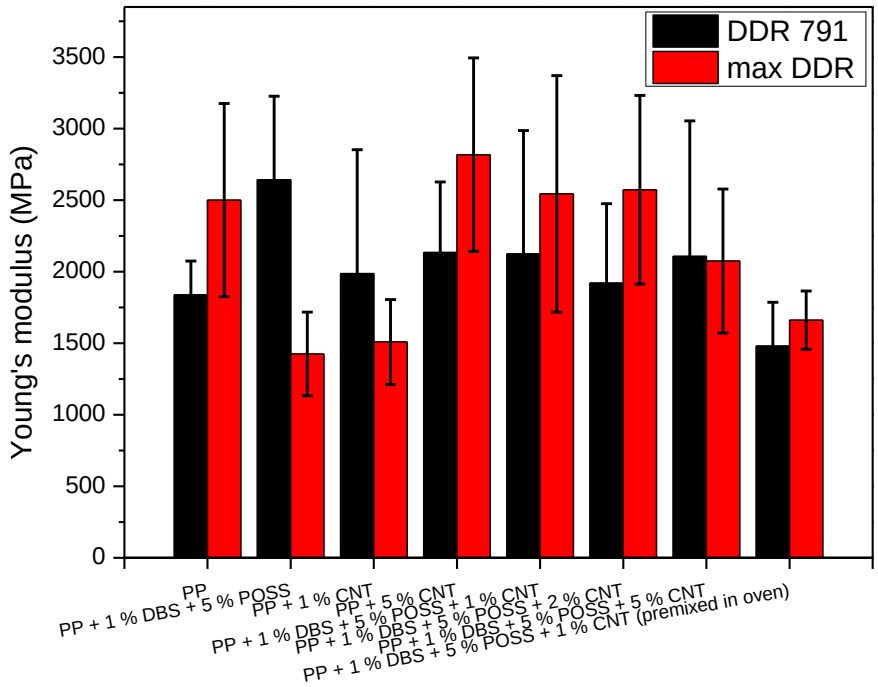

Fig. 4.8 Young's modulus of different iPP/DBS/POSS/CNT nanocomposites

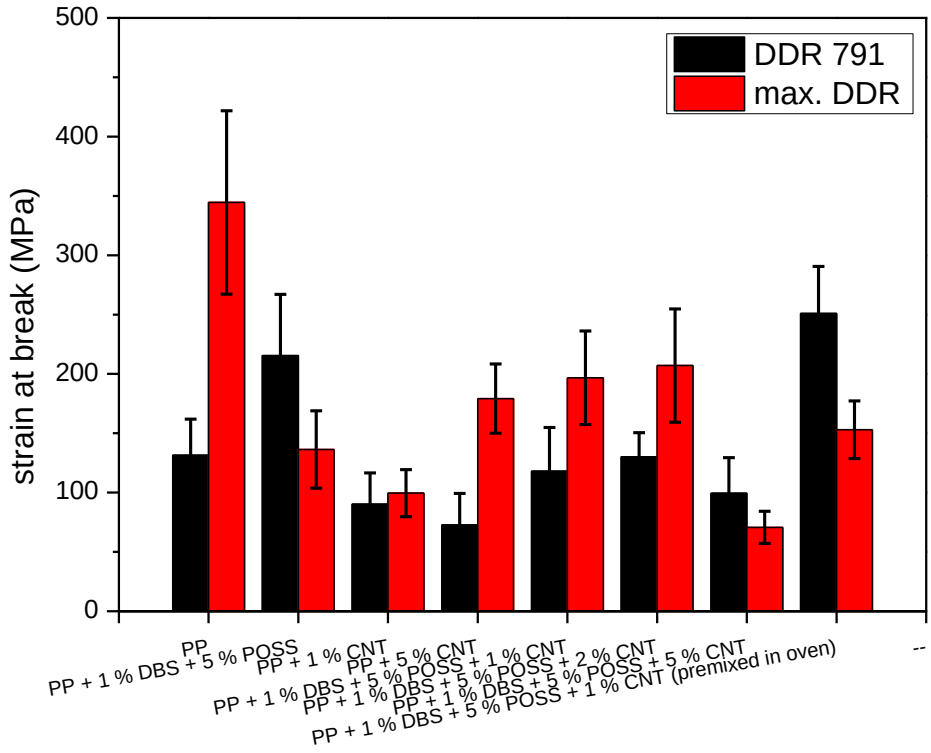

Fig. 4.9 Strain at break of different iPP/DBS/POSS/CNT nanocomposites

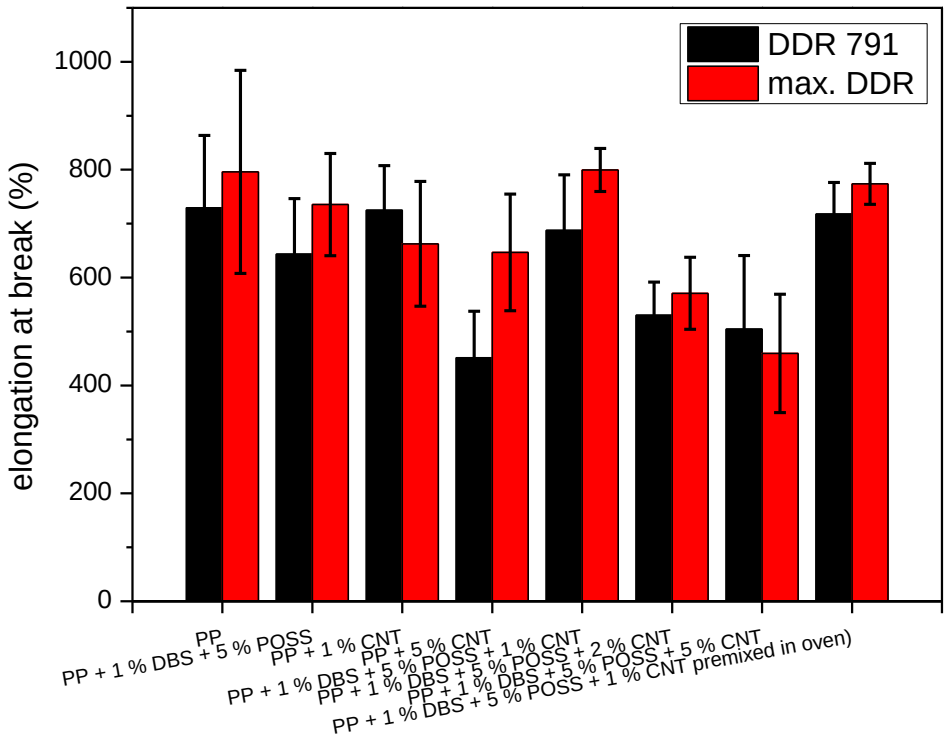

Fig. 4.10 Elongation at break of different iPP/DBS/POSS/CNT nanocomposites

4.5 Thermal Properties

Thermal properties can give information about processing parameters, crystallization behavior and allows conclusions on the morphology of the PNC. The calculated crystallinities of the different iPP/DBS/tri-POSS compounds containing different amounts of CNT, silica and nanosilicon are shown in Fig 4.11. For all produced compounds the crystallinity in the heating run, as well as in the cooling run, show only minor deviations from the values of unfilled iPP. Therefore no clear trend can be seen from these results. Fig. 4.12 depicts the melting temperature and the crystallization temperature of the investigated nanocomposite. None of the used fillers has a significant influence on the melt temperature of the compound. For all filled specimens an increase in the crystallization temperature can be observed, compared to the crystallization temperature of iPP. The measured fibers show the same trend as the melt mixed compounds (see Fig. 4.12 and Fig. 4.13). The combination of increasing melt temperatures and no change of crystallinity is because the nanofillers are nucleating smaller polypropylene crystals at higher temperatures [Assouline et al (2003); Sandler et al. (2003); Xia et al. (2004)]. The

fibers filled with silica and nanosilicon were not measured with DSC due to the end of the research stay.

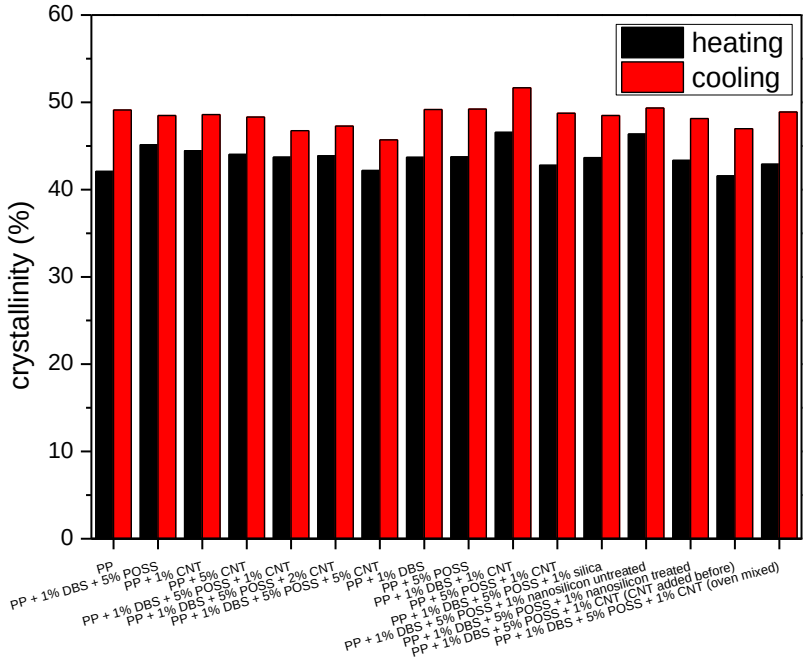

Fig. 4.11 Crystallinities of different nanocomposites (melt mixed)

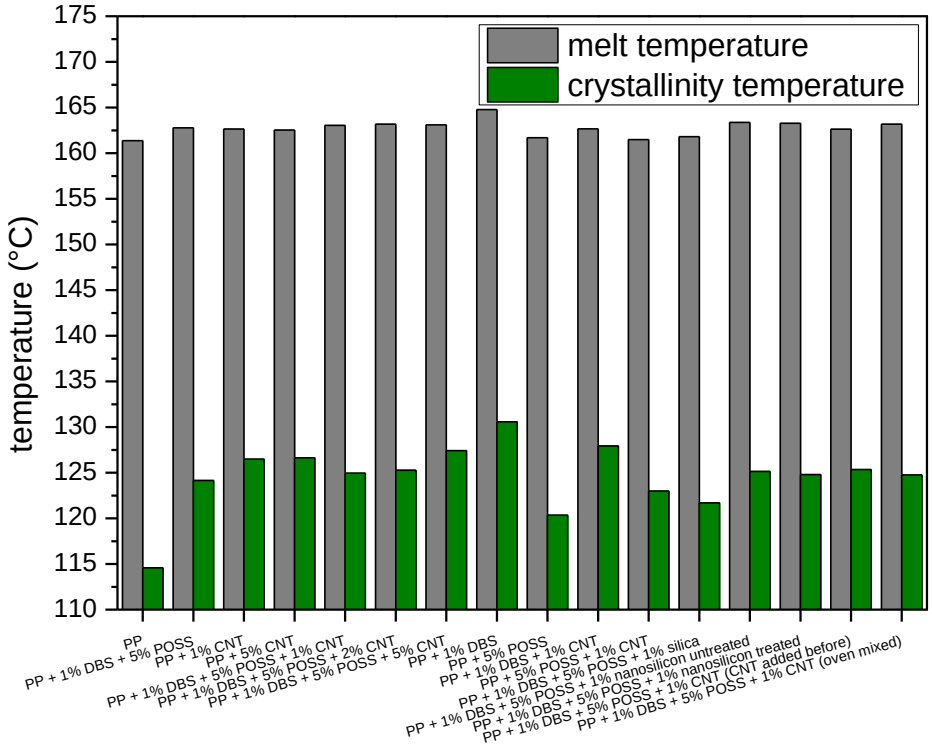

Fig. 4.11 Melt and crystallization temperatures of different nanocomposites (melt mixed)

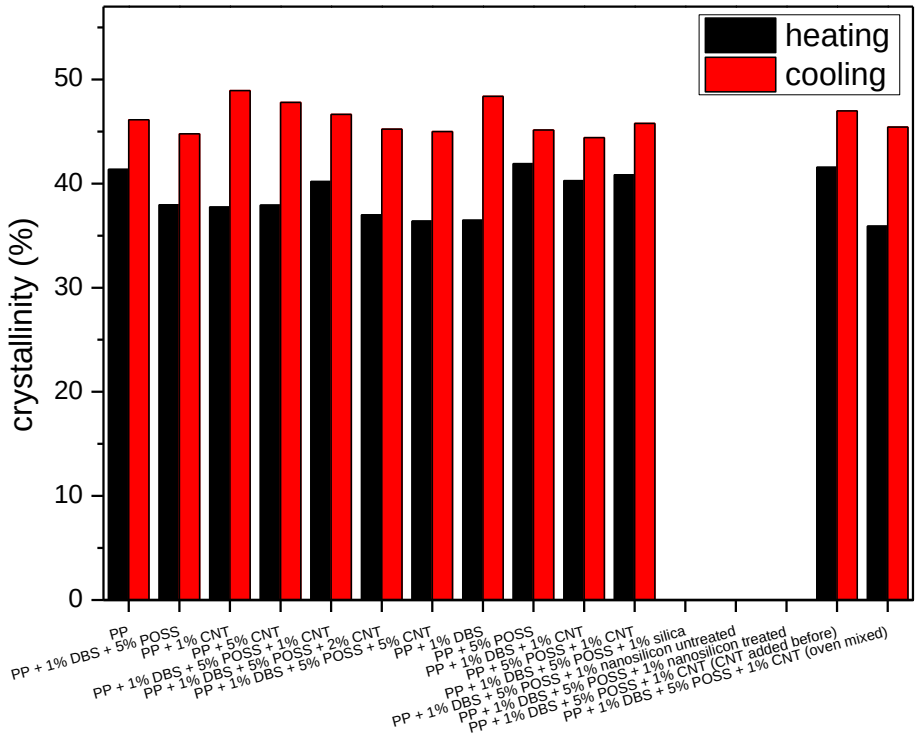

Fig. 4.12 Crystallinities of different nanocomposites fibers (DDR 791)

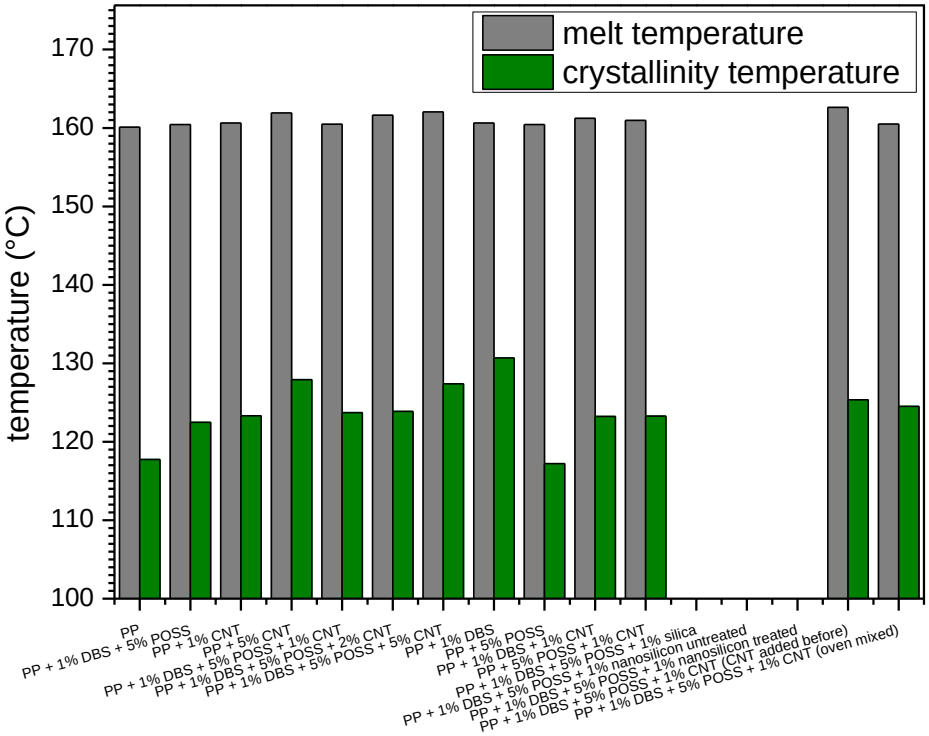

Fig. 4.13 Melt and crystallization temperatures of different nanocomposites fibers (DDR 791)

4.6 Polarized Cross Microscope

The optical microscope in polarized mode can show different structural states such as DBS fibrils or crystals. Due to the low magnification of 100x no such structures could be observed. Optical microscope images of iPP/DBS/tri-POSS compound filled with 1 wt% CNT at three different temperatures (25, 120, 210 °C) are shown for the reason of completeness in Fig. 4.14. In the vicinity of the big structure on the right side in the 120 °C some residuals of the low viscosity liquid complex can be observed, which are formed during cooling. They appear as light grey circular shaped particles inside the matrix surrounding the particle. The large structure in the middle is supposedly a crystalline domain. With advanced magnification of the optical microscope more information about the structural formations inside of iPP/DBS/tri-POSS compounds could be generated.

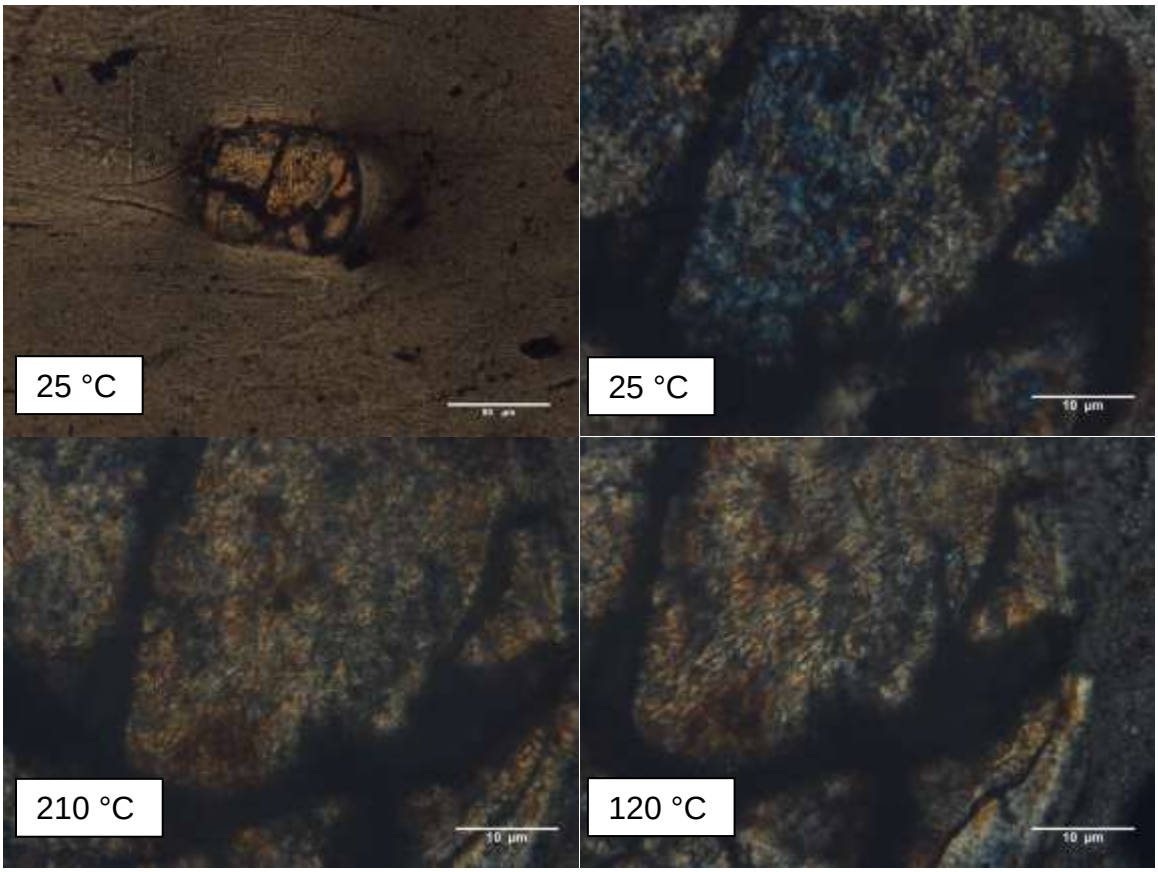

Fig. 4.14 Optical microscope images of iPP / 1 wt% DBS / 5 wt% POSS / 1 wt% CNT nanocomposite

4.7 Transmission electron microscope

For better understanding of the interactions between DBS, POSS and CNT transmission electron microscope (TEM) images were taken (see Fig. 4.15). Due to the limited time of the research stay no images could be taken of DBS, POSS and silica or DBS, POSS and nanosilicon solutions. Fig. 4.15 a and Fig. 4.15 b show agglomerated CNT. Several structures could be found in the DBS/POSS/CNT (1:5:1.2) solution (see Fig. 4.15 c-e). Without further characterization methods is not clear to identify the different particles. It was not possible to find particles which can clearly contributed to DBS or POSS or the low viscosity liquid complex.

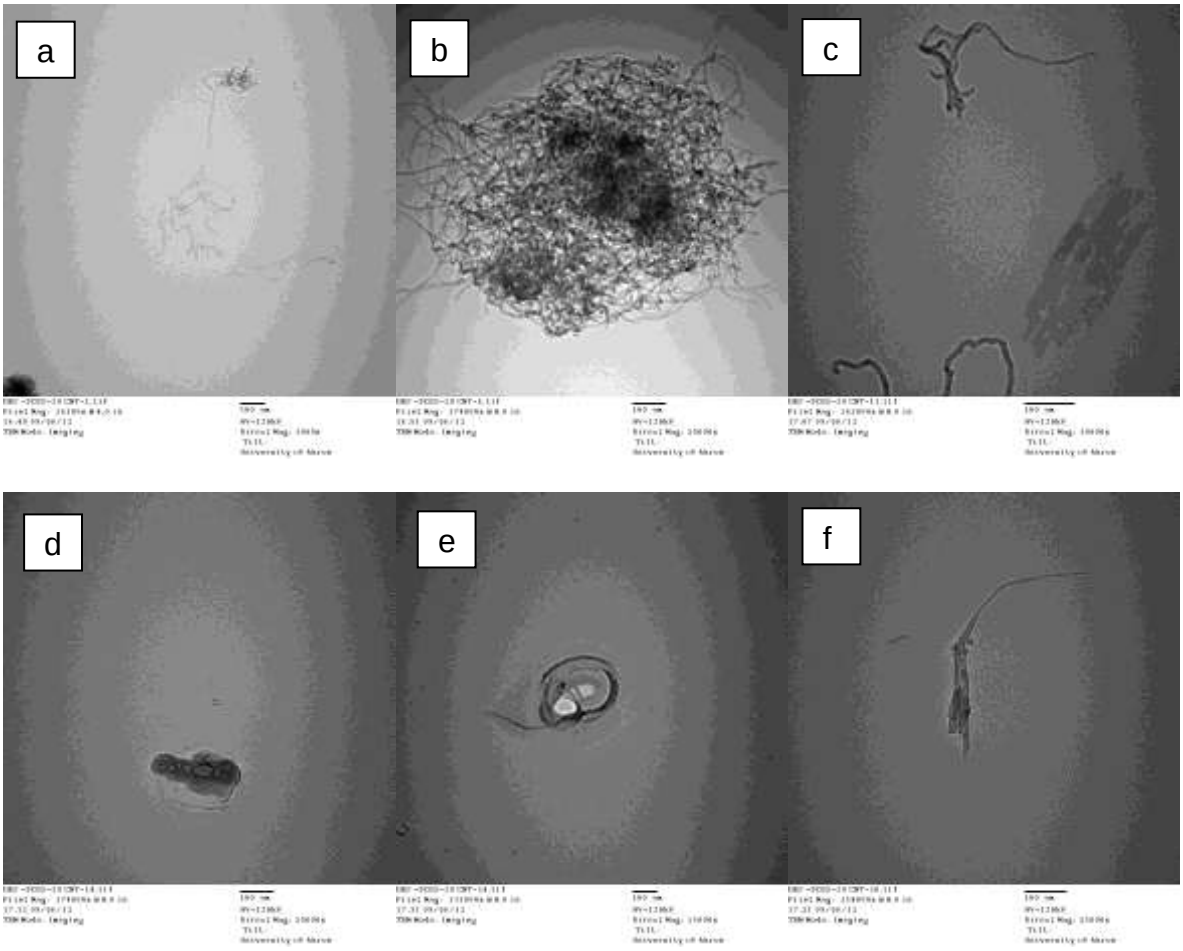

Fig. 4.15 TEM images of solution mixed DBS/POSS/CNT (1:5:1.2)

4.8 Scanning electron microscope

In this chapters scanning electron microscope (SEM) images were taken from mixed nanofillers and nanocomposites fibers with different DDR. The morphology of DBS/tri-POSS/CNT (1:5:1.2) solution based mixture is shown in Fig. 4.16. It can be

seen that tri-POSS forms a crystalline structure different from what was observed in DBS/tri-POSS complex [Roy et al. (2012); Roy et al. (2011)]. The image confirms that the presence of CNT disturbed the formation of the DBS/tri-POSS complex. This corroborates the trend seen in the rheological properties and in DDR.

The SEM image of DBS/tri-POSS/nSi (1:5:1.2) shows that nanosilicon particles formed agglomerates (see Fig. 4.17). The morphology for DBS/tri-POSS/silica (1:5:1.2) is comparable with that of DBS/tri-POS/nSi (1:5:1.2), which can be seen in Fig. 4.18.

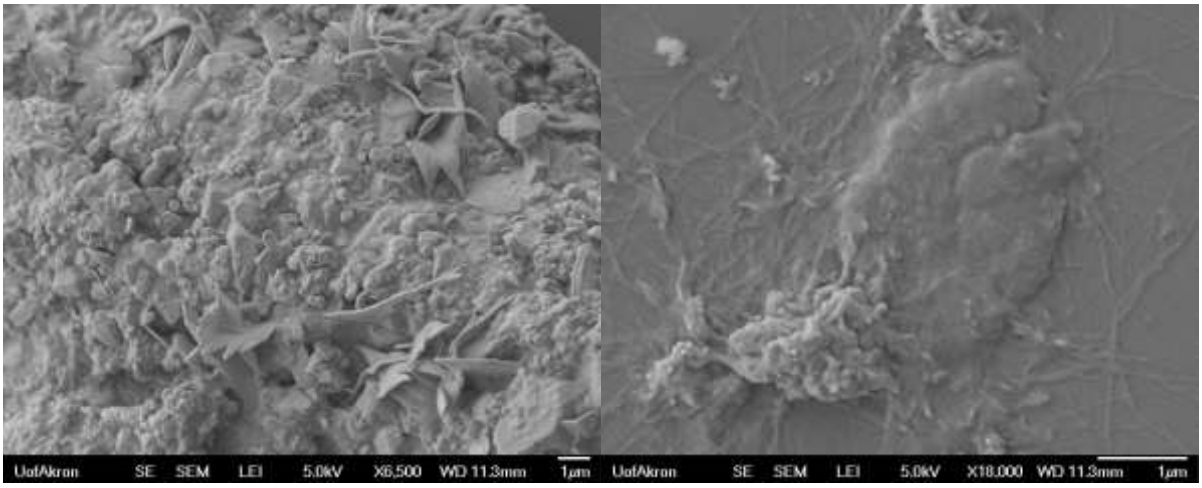

Fig. 4.16 SEM image of DBS/POSS/CNT (1:5:1.2) solution

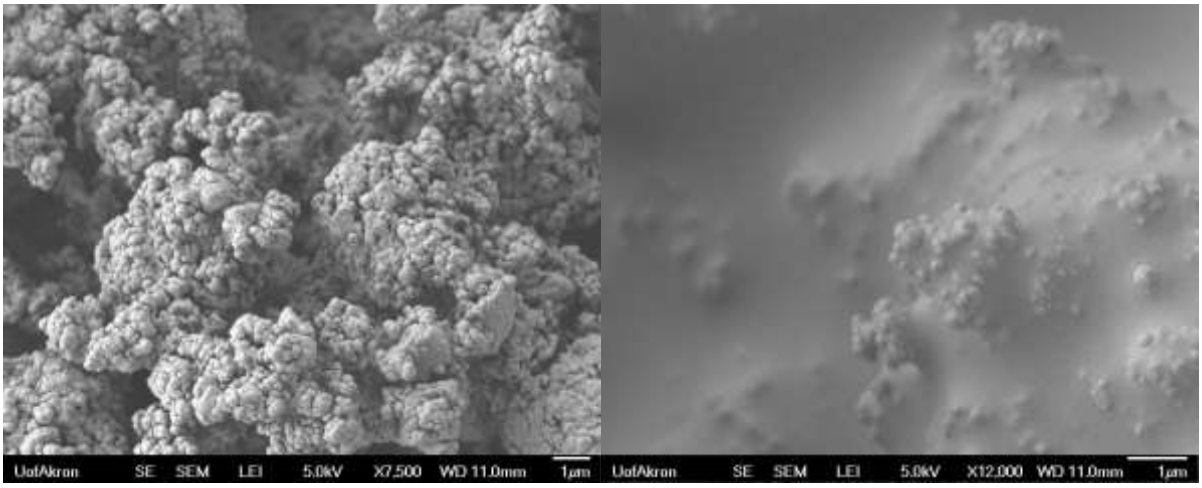

Fig. 4.17 SEM image of DBS/POSS/nanosilicon (1:5:1.2) mixed in the oven for 5 min at 190 °C

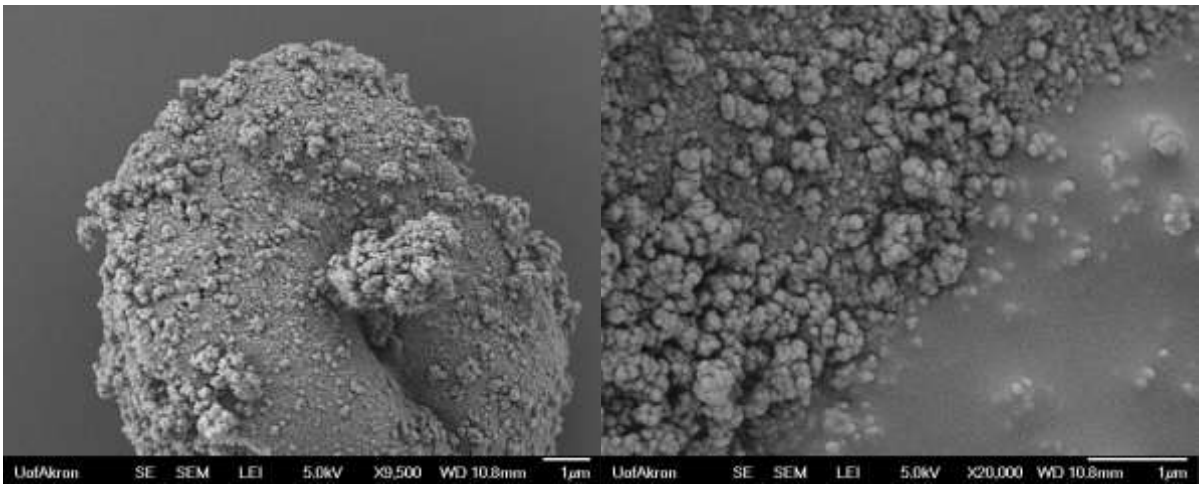

Fig. 4.18 SEM image of DBS/POSS/silica (1:5:1.2) mixed in the oven for 5 min at 190 °C

The morphology of iPP / 1 wt% DBS / 5 wt% POSS / 1 wt% CNT nanocomposite spun fibers (DDR 119) without epoxy preparation can be observed in Fig. 4.19. It can be seen that the agglomerates of CNT on the surface of the fibers.

SEM images of the spun fiber with the composition of iPP / 1 wt% DBS / 5 wt% POSS / 1 wt% CNT (DDR 119) shows that the CNT remained as agglomerates and that DBS/tri-POSS formed numerous short particles of cylindrical shape with a diameter of about 500 nm (see Fig. 4.20). This is in contrast to long cylindrical particles of DBS/tri-POSS with typical diameter of 100 nm. With increasing DDR the cylindrical shaped particles becomes longer due to the applied force during fiber spinning (see Fig. 4.21 and Fig. 4.22). This confirms the results in literature [Roy et al. (2012)]. The same trend can also be observed with increased CNT content (see Fig. 4.23 – Fig. 4.25).

Combining the trend of shear viscosity data and size of DBS/tri-POSS SEM image in Fig. 4.23, it can be inferred that DBS and tri-POSS molecules were able to form complex even in the presence of CNT, but the extent was much less than when CNT was not used. This poses an interesting question – what factors are responsible for disturbance of DBS/tri-POSS complex formation when other nanofillers are used. Such question is an interesting topic for a future study.

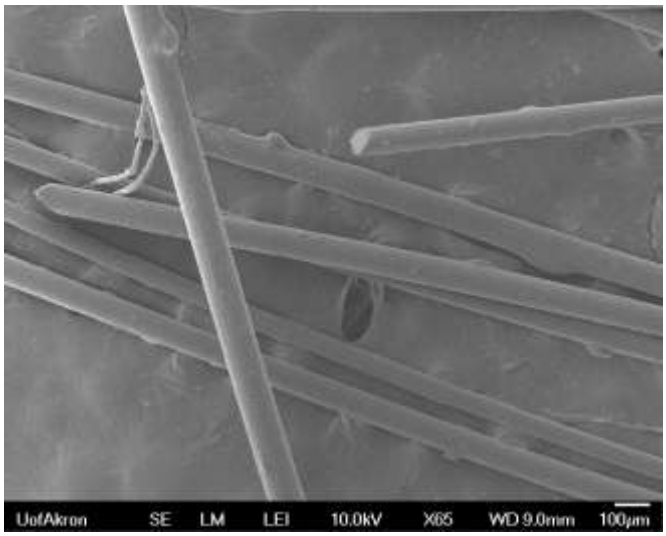

Fig. 4.19 SEM image of iPP / 1 wt% DBS / 5 wt% POSS / 1 wt% CNT fibers (DDR 119)

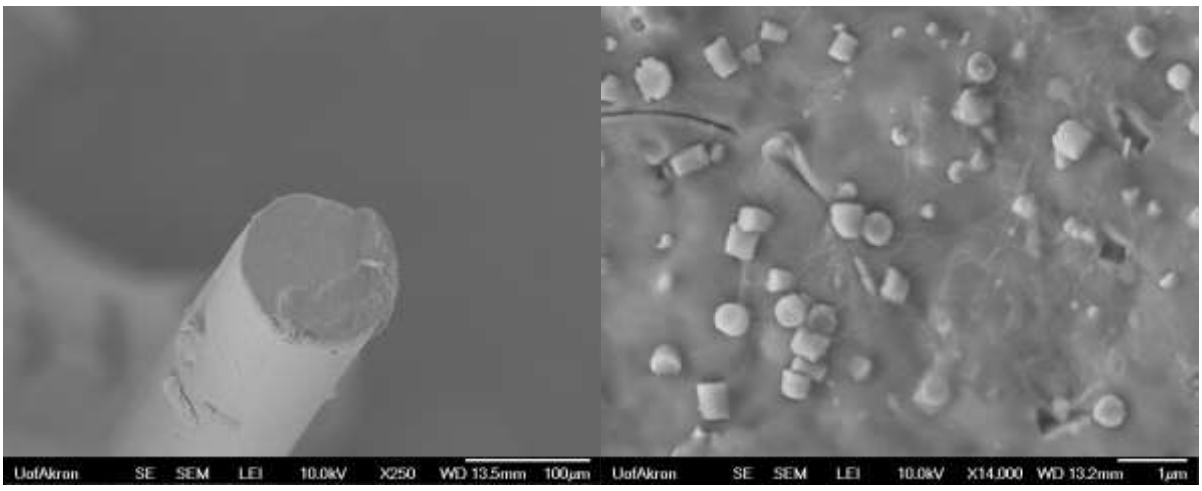

Fig. 4.20 SEM image of iPP / 1 wt% DBS / 5 wt% POSS / 1 wt% CNT fibers (DDR 119)

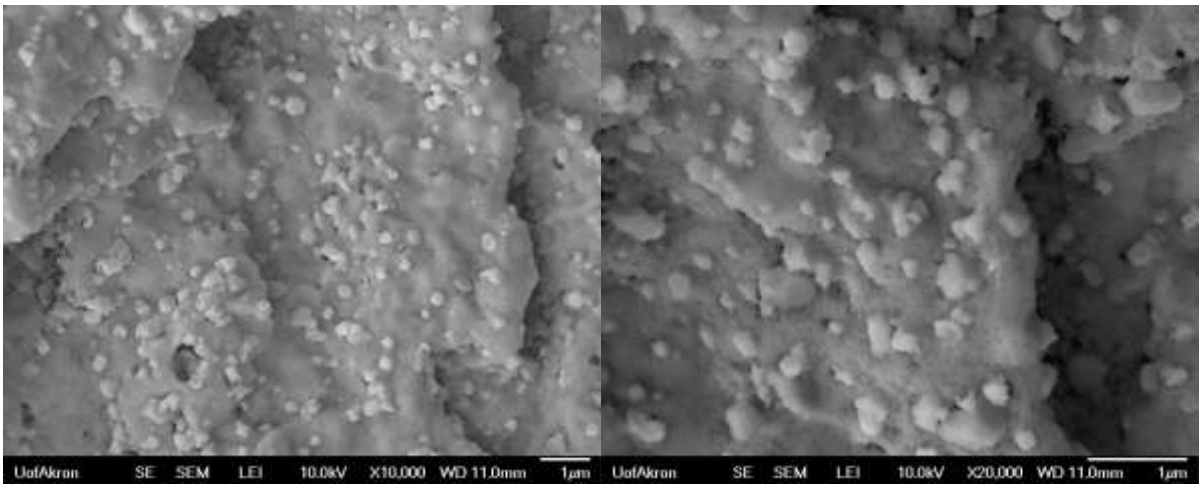

Fig. 4.21 SEM image of iPP / 1 wt% DBS / 5 wt% POSS / 1 wt% CNT fibers (DDR 791)

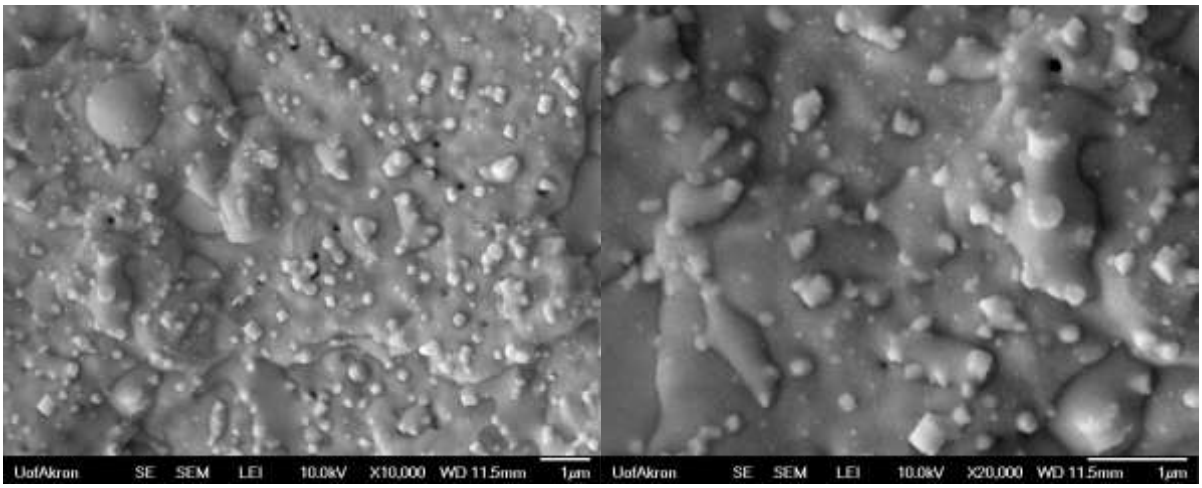

Fig. 4.22 SEM image of iPP / 1 wt% DBS / 5 wt% POSS / 1 wt% CNT fibers (DDR 1140)

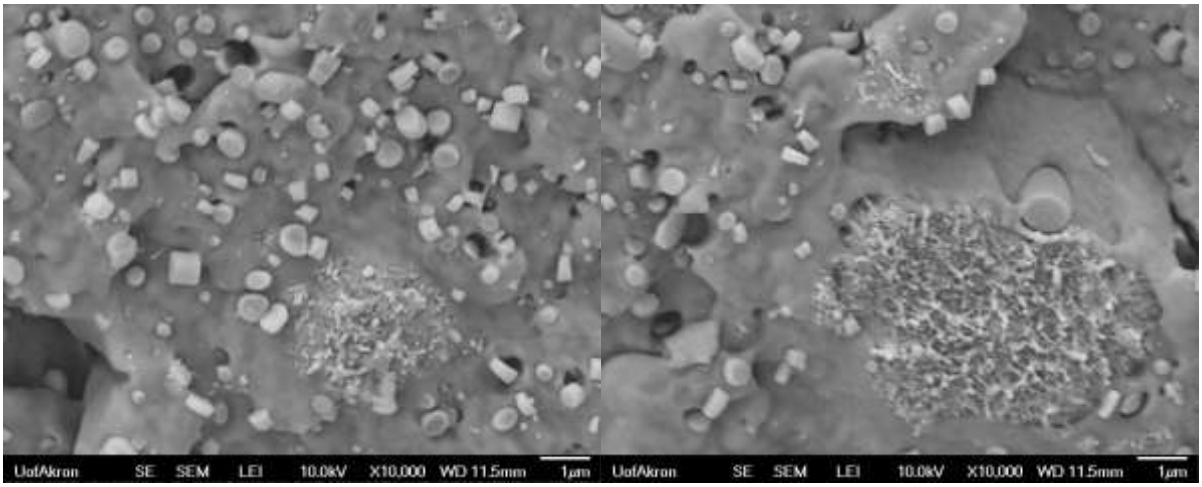

Fig. 4.23 SEM image of iPP / 1 wt% DBS / 5 wt% POSS / 2 wt% CNT fibers (DDR 119)

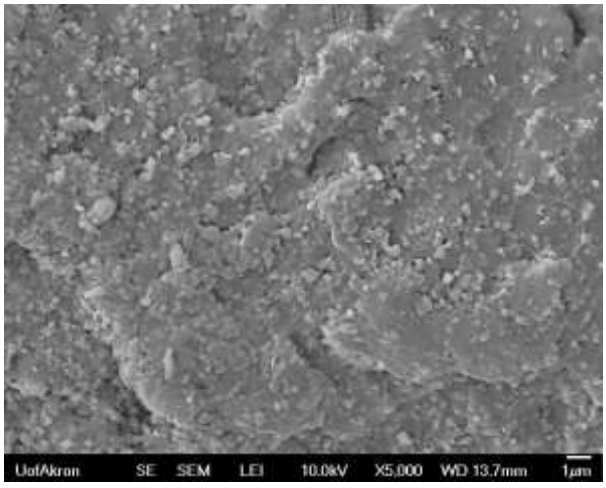

Fig. 4.24 SEM image of iPP / 1 wt% DBS / 5 wt% POSS / 5 wt% CNT fibers (DDR 119)

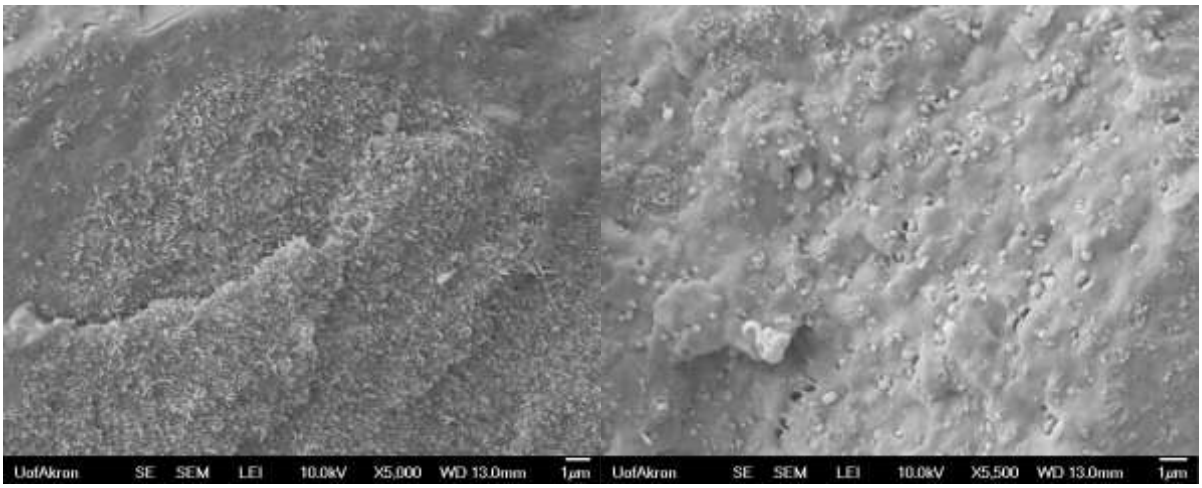

Fig. 4.25 SEM image of iPP / 1 wt% DBS / 5 wt% POSS / 5 wt% CNT fibers (DDR 791)

4.9 X-ray photoelectron spectroscopy

The X-ray photoelectron spectroscopy (XPS) were used to identity chemically the surface of the material. Furthermore the chemical bonding of the sample can be analyzed. CNTs show only one peak, which can be contributed to C 1s bond. So there are no other functional groups, which can be used for the interactions with the other nanofillers. For the unmodified CNT a modification could be used to establish better interactions between the single components.

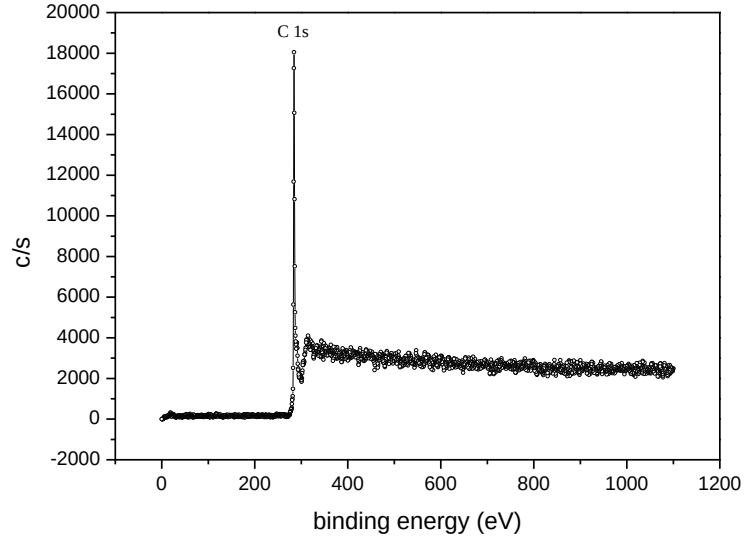

Fig. 4.26 Survey of CNT powder

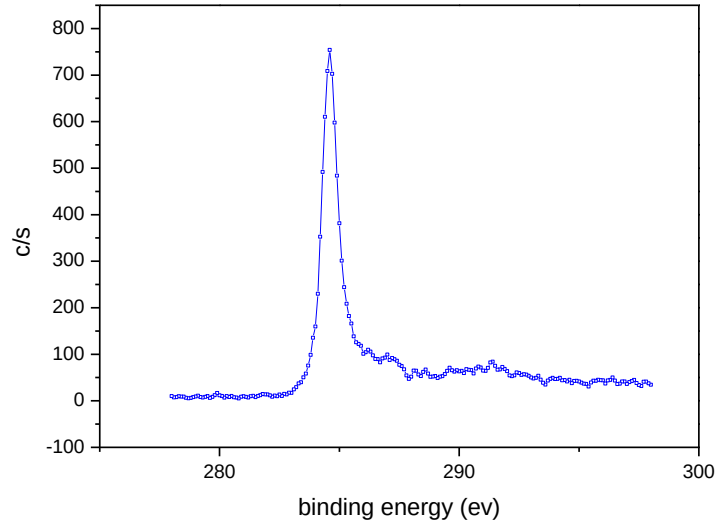

Fig. 4.27 C1s of CNT powder

4.10 Orientation factor and crystallinity via WAXD

The Herman orientation was calculated for the a-, b- and c-axis of the monoclinic iPP crystals. Unity describes perfect parallel orientation, zero specifies random orientation and perpendicular orientation is identified by -0.5. The results are not complete due to the limited time of the research stay.

The orientation factor fa is depicted in Fig. 4.28. No clear trend of filled nanocomposites with increased DDR can be found. Presumably this is also due the agglomeration of nanofillers. The orientation varies from nearly random orientation to slight perpendicular orientation.

The trend for the orientation factor fb of various nanocomposites is increased with increased DDR (see Fig. 4.29). A more perpendicular orientation can be seen.

In Fig. 4.30 the orientation factor fc for all fibers at 3 different DDR are displayed. With the addition of the various filler the orientation factor changes to a more random morphology. With higher DDR a more random orientation can be seen.

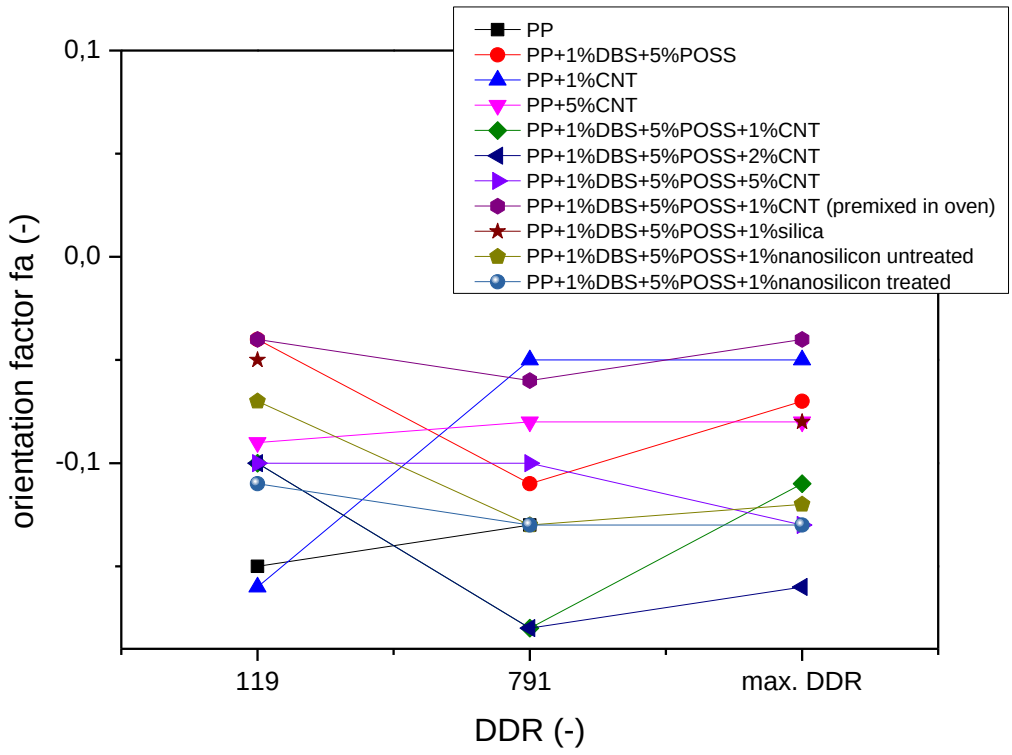

Fig. 4.28 Orientation factor fa of different nanocomposites in dependency of DDR

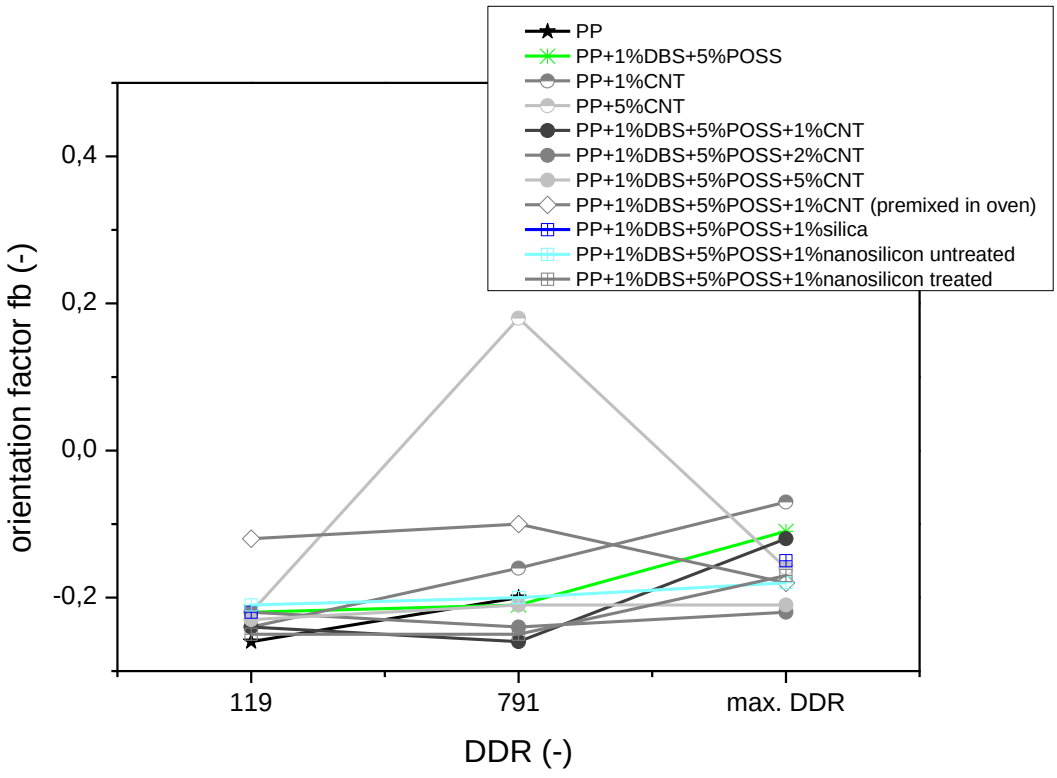

Fig. 4.29 Orientation factor fb of different nanocomposites in dependency of DDR

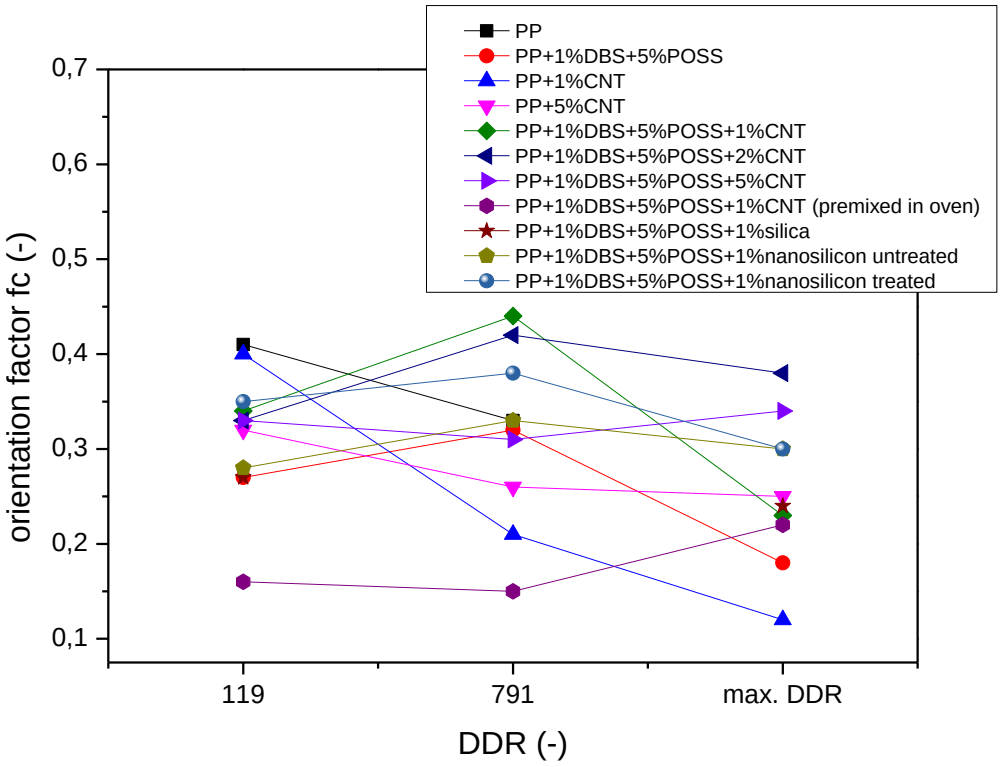

Fig. 4.30 Orientation factor fc of different nanocomposites in dependency of DDR

With the help of WAXD the crystallinity can be measured. The results are not complete because of the limited duration of the research stay. It can be seen that with increasing DDR the crystallinity increases too (see Fig. 4.31). Also the crystallinity is higher than that measured with DSC. According to literature the calculation of the crystallinity via WAXD measurements provides more accurate crystallinity values for deformed materials compared to calculation method via DSC. The DSC method does not reproduce the real crystallinity of the fibers due to the inherent heating process, which causes a relaxation and change in the crystallinity of the fibers and a different intrinsic equilibrium state [Lima et al. (2002)]. For all produced compounds the calculated crystallinity is rather uniform with values from 65 to 75 %, whereby the highest values were achieved by iPP/DBS/tri-POSS compound containing silica and the lowest by iPP compound containing 5 wt% CNT. For the compounds containing CNT there is no clear trend observable regarding the increase of crystallinity with higher DDR.

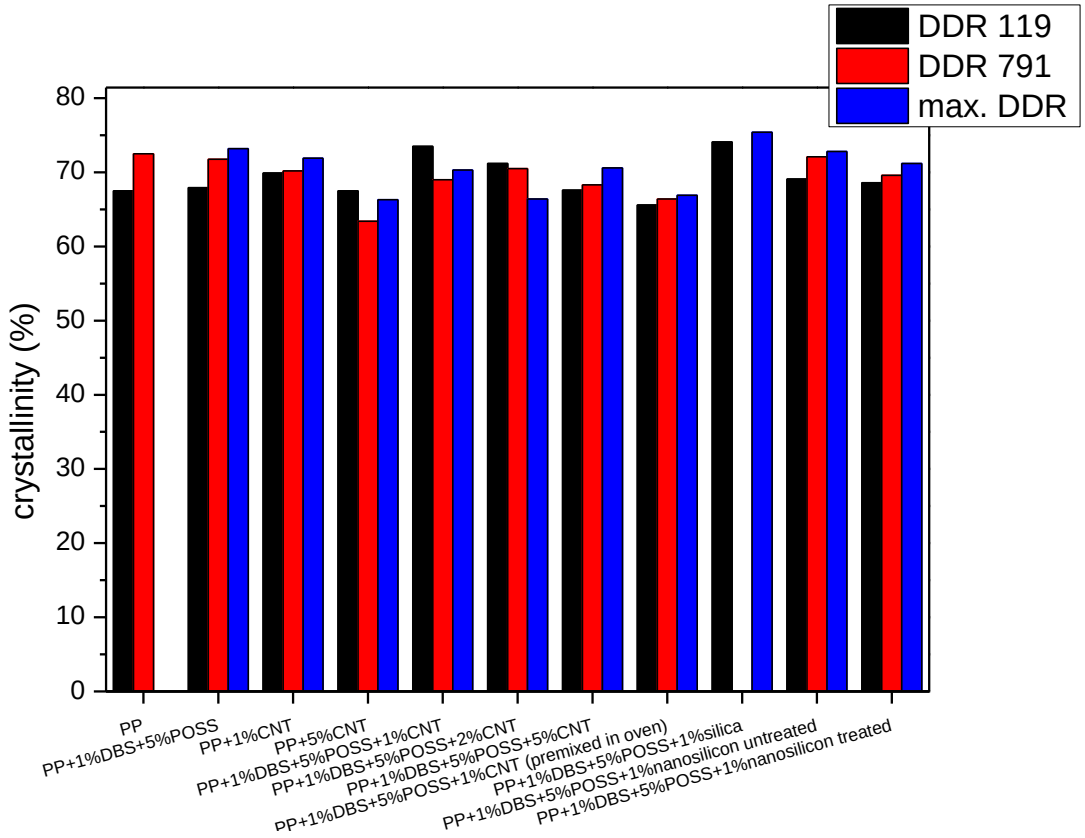

Fig. 4.31 Calculated crystallinity via WAXD of different iPP nanocomposite fibers

5 POSSIBLE FURTHER RESEARCH WORKS

The results show that there is still great potential for modification of nanofillers. In this chapter some possibilities for modifications are presented. CNT tend to agglomerate due to their geometric shape and strong van der Waals force attraction [Han and Fina (2011); Qian et al. (2000)]. The chemical modification can be divided into the involvement of the π-conjugated skeleton of CNTs in chemical reaction with various reagents and into the adsorption of various molecules through non-covalent interaction (see Fig. 5.1) [N. Roy et al. (2012)].

Regarding the enhancement of homogenous dispersion of CNT in the polymer matrix several ways such as modification of CNT such as end-group functionalization [McIntosh et al. (2006); McIntosh et al. (2007); Zhou et al. (2007)], use of ionic surfactants [Vaisman et al. (2006)], plasma coating [Shi et al. (2003)], shear mixing [Lopez Manchado et al. (2005); Xiao et al. (2007)] or adding of other nanofiller can be used. The compatibility between polypropylene and fillers can be improved with matrix modification by grafting it with reactive moieties such as acrylic acid, acrylic esters or maleic anhydride [Kelarakis et al. (2006); Zhou et al. (2006)], which leads to enhancement in thermal and electrical properties of polypropylene CNT nanocomposites [Tjong et al. (2007); Jiang et al. (2006); Lee et al. (2007)]. Especially maleic anhydride can improve the dispersion and the properties of PP/MWCNT nanocomposites due to strong hydrogen bonding between hydroxyl groups of MWCNT and maleic anhydride groups of the compatibilizer [Lee et al. (2008)]. Chemical modifications have also drawbacks. They can attack the surface of CNT and therefore reduces their mechanical properties.

Covalent functionalization can improve the homogenous dispersion of CNT. Oxidation [Liu et al. (1998); Xu et al. (2006)], atom transfer radical polymerization [Shanmugharaj et al. (2007); Gao et al. (2007)], acylationmediated amidation [Chen et al. (1998); Peng et al. (2003)] and carbodiimide-activated coupling [Williams et al. (2002); Ogino et al. (2006)] are commonly used functionalizing methods [Lan and Lin (2009)]. But these methods can destroy the sp2 structure in the graphite sheet due to the covalent bonding reaction.

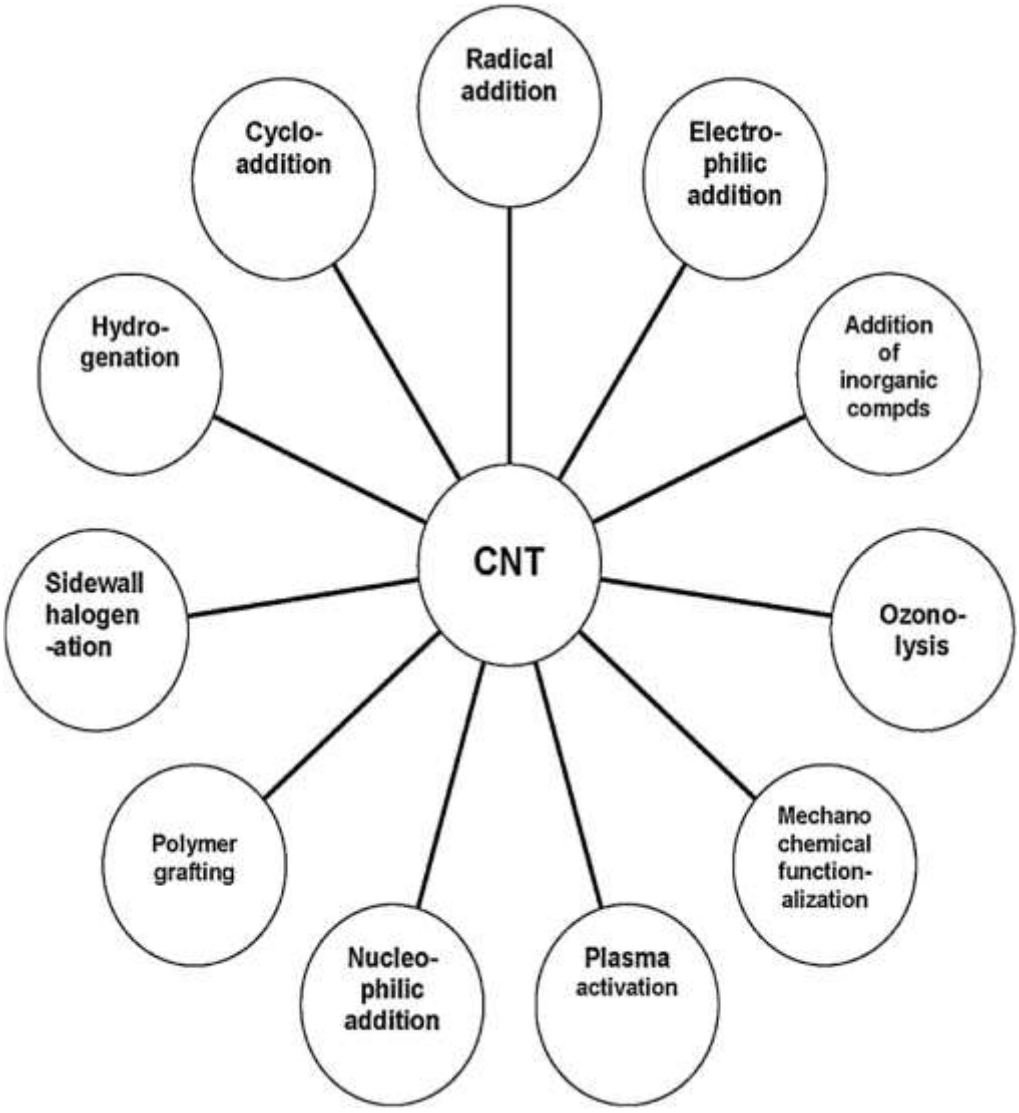

Fig. 5.1 Different modifications methods [N. Roy et al. (2012)]

Fukushima et al. (2003) and Price et al. (2005) found out that room temperature ionic liquids are effective for dispersing CNTs by physical grinding to form gels through cation-π interaction.

Lan and Lin (2009) showed that with addition of mineral fillers such as layered silicates or LDH the aggregation behavior of CNT could be decreased. With the addition of layered silicates they could increase the CNT dispersion significantly. Also good results could be achieved with mica and layered double hydroxide (LDH). They only grinded the CNTs and the mineral filler physically into fine powder and dispersed in different solution (water and toluene).

Chen and Shimizu (2008) combined acyl-chloride-functionalized-MWCNT and amino-propyl-isooctyl-POSS via amide linkages. The prepared amino-propyl-isooctyl-POSS

modified MWCNT (MWCNT-g-POSS) could be dispersed homogenously in poly(L-lactide.

Gomathi et al. (2010) showed the octa-tetra-methyl-ammonium-POSS is a good reagent for covalent functionalization of metal oxides and nanocarbons. By Acid treatment surface hydroxyl and carboxyl groups were generated.

Zhang et al. (2010) reacted amino-propyl-isobutyl-POSS with MWCNT–COOH (surface bonded acyl chloride moieties) to a new soluble material. So the processability of MWCNT was enhanced significantly (see Fig. 5.2).

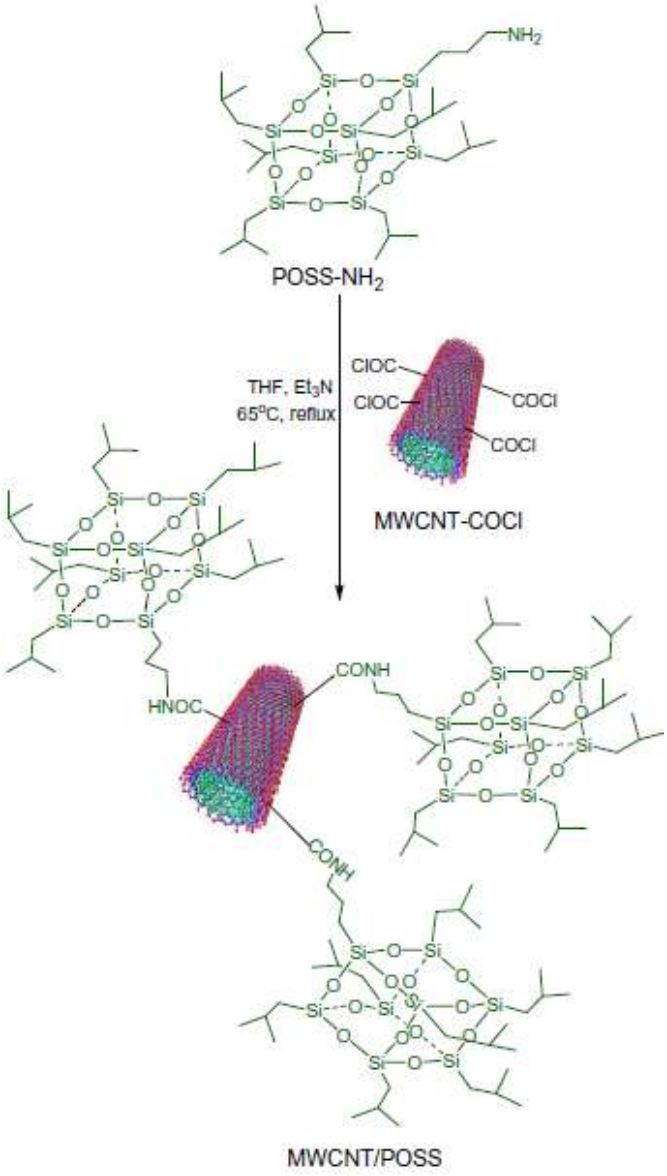

Fig. 5.2 MWCNT modified with POSS [Zhang et al. (2010)]

There are a lot of possibilities to improve the interaction between iPP, DBS, POSS and other nanofillers. Further research work of modification and processing should be done to get an adequate property profile of iPP/DBS/POSS/nanofiller nanocomposites.

6 CONCLUSION

This research work investigated the influence of different nanofillers on the formation of low viscosity liquid complex of DBS and tri-POSS in nanocomposites with iPP. The processing technique has a main influence on the complete formation of the low viscosity liquid complex of POSS and DBS. Especially the premixing method in combination with CNT showed different behavior compared to the conventionally prepared sample of the same composition. The formation of the low viscosity liquid complex is crucial to the final properties of the compound but has its main impact on the rheological properties and thereby also on the achieved dispersion of an additional nanofiller such as CNT.

The SEM image clearly indicates that nanocomposites of iPP with DBS/tri-POSS/CNT contain agglomerated CNT. The DBS/tri-POSS particles are of much larger diameter than those in the absence of CNT. Also the silica and treated respectively untreated nanosilicon particles tend do agglomeration. This trend to agglomeration of the nanoparticles shall be overcome to achieve better performance of the compounds is many aspects. This might be achieved with modification or functionalization of the nanoparticles to achieve better compatibility and dispersion inside the polymeric matrix.

The slight shoulder in the complex viscosity curve of iPP/DBS/tri-POSS compounds indicated the DBS fibrillar network formation inside of the compound. Thus, in the presence of CNT and nanosilicon, the formation of the low viscosity liquid complex is disturbed by the nanoparticles and is therefore not complete. The iPP/DBS/tri-POSS nanocomposite containing nanosilicon show a huge shoulder at about 160 °C in the complex viscosity curve, which indicates significantly an even more disturbed formation of the low viscosity liquid complex and the formation of DBS fibrils.

The measured maximum draw down ratios show the processability of the nanocomposites regarding fiber spinning. The addition of CNT, nSi and silica to the iPP/DBS/tri-POSS compounds caused a reduction of DDR, but such values are still higher than unfilled iPP. The premixing of DBS and POSS leads to a further decreased maximal DDR value, but remains still higher than unfilled PP. Supposedly

the low viscosity liquid complex is not formed properly by this technique. The treatment of nanosilicon improves the properties of the filler so a maximum DDR comparable to the values of unfilled iPP/DBS/tri-POSS compounds can be achieved. Presumably the surface treatment of the nanosilicon improves the mutual interaction between the filler and the iPP/DBS/tri-POSS compound and enhances thereby the fiber spinning properties.

The mechanical properties of iPP/DBS/tri-POSS compounds are heavily influenced by the addition of the nanoparticles. The increase of CNT content in the iPP/DBS/tri-POSS compound reduces the Young's modulus. None of the produced compounds could achieve strain at break values like unfilled iPP. Too high content of CNT and wrong production technique has a massive influence on the strain at break values. The elongation at break values shows rather uniform values for all iPP/DBS/tri-POSS compounds with and without CNT as filler, except for the highest contents of CNT.

The crystallinity of the produced nanocomposite shows only insignificant deviation from the values achieved by unfilled iPP. Also the melting temperature alters only within a small range. For all filled specimens an increase in the crystallization temperature can be observed, compared to the crystallization temperature of iPP. The measured fibers show the same trend as the melt mixed of iPP/DBS/tri-POSS compounds containing nanofillers.

The possibilities to change the property profile of nanocomposites by influencing the interaction between polymer, DBS, POSS and other nanofillers are very huge. Still more research work has to be done, to establish clear relationships between composition, processing and the resulting property profile of the nanocomposite.

7 ACKNOWLEDGE

First of all, I want to acknowledge Prof. Jana and his fantastic work group for the stay at the Department Polymer Engineering (The University of Akron). Prof. Jana offered me a challenging research topic, had a permanent interest in my work and the discussions with him helped me to have a different look on my research.

I am also very grateful to Prof. Holzer for supporting me in my research work, which has been beneficially for this research report.

My colleagues at the University of Akron help me with different characterization methods, the according sample preparation and their suggestions. Especially I want to thank Dr. Sayantan Roy, Dr. Rong Bai, Dr. Sritama Kar, Kushal Bahl, Xiao Wang, Rafael Benavides Gonsalez, Eric McClanahan, Karen Jackson, Jeff Long, Sepideh Niknezhad, Maher Al Rashed, Shenlong Gu, Jon Page, Ila Badge and many more.

I also want to thank the Marshall Plan Scholarship which gave me the unique opportunity to research in a foreign country.

8 REFERENCES

Adachi, H., Hyashi, O., Okahashi, K. (1990). Japanese Patent Kokoku **H 2 15863**.

Adachi, H., Hayashi, O., Okahashi, K. (1985). Japanese Patent Kokai **S 60 108841**.

Adachi, H., Adachi, E., Hayashi, O., Okahashi, K. (1992). Japanese Patent Kokoku **H 4 56975**.

Adachi, H., Adachi, E., Aiba, Y., Hayashi, O. (1990). Japanese Patent Kokai **H 2 222537** and U.S. Patent **5087553**.

Afshari, M., Kotek, R., Gupta, B.S., Kish, M.H., Dast, H.N. (2005). Journal of Applied Polymer Science **97**, 532.

Ajayan, P.M. (1999). Chemical Reviews **99**, 1787.

Alexander, L.E. (1969). In “X-ray Diffraction Methods in Polymer Science”, John and Wiley & Sons Inc., New York.

Alexandre, M., Beyer, G., Henrist, C., Cloots, R., Rulmont, A., Jerome, R., Dubois, P. (2001). Macromolecular Rapid Communications **22**, 943.

Alzari, V., Mariani, A.,m Monticelli, O.,Valentini, L., Nuvoli, D., Piccinini, M. (2010). Journal of Polymer Science Part A: Polymer Chemistry **48**, 5375.

Ambronn, H., Zsigmondy, R. (1899). Berichte über die Verhandlungen der Königlich-Sächsischen Gesellschaft der Wissenschaften zu Leipzig **51**, 13.

Ambronn, H. (1896). Berichte über die Verhandlungen der Königlich-Sächsischen Gesellschaft der Wissenschaften zu Leipzip **8**, 613.

Andrianov, K.A. (1938). Russian Journal of General Chemistry **17**, 1522.

Andrianov, K.A. (1946). Russian Journal of General Chemistry **16**, 633.

Arai, M., Kanamaru, M., Matsumura, T., Hattori, Y., Utsumi, S., Ohba, T., Tanaka, H., Yang, C.M., Kanoh, H., Okino, F., Touhara, H., Kaneko, K. (2007). Adsorption **13**, 509.

Ardanuy, M., Velasco, J.I. (2011). Applied Clay Science **51**, 341.

Assouline, E., Lustiger, A., Barber, A.H., Cooper, C.A., Klein, E., Wachtel, E., Wagner, H.D. (2003). Journal of Polymer Science Part B – Polymer Physics **41**, 520.

Azuma, K., Shindo, Y., Ishimura, S. (1982). Japanese Patent Kokai **S 57 56820**.

Imai, E., Takeno, H. (1984). Japanese Patent Kokai **S 59 129939**.

Barrey, A.J., Daudt, W.H., Domicone, J.J., Gilkey, J.W. (1955). Journal of the American Chemical Society **77**, 4248.

Bethune, D.S., Kiang, C.H., DeVries, M.S., Gorman, G., Savoy, R., Beyers, R. (1993). Nature **363**, 605.

Beyer, G. (2002). Fire and Materials **26**, 291.

Bharat, B. (2010). In "Springer Handbook of Nanotechnology", 3rd ed., Berlin, Germany.

Bikiaris, D., Vassiliou, A., Chrissafis, K., Parakevopoulos, K.M., Jannadoudakis, A., Docoslis, A. (2008). Polymer Degradation and Stability **93**, 952.

Balzano, L., Portale, G., Peters, G.W.M. (2008). Macromolecules **41**, 5350.

Bordere, S., Copart, J.M., El Bounia, N.E., Gaillard, P., Passade-Boupat, N., Piccione, P.M., Plee, D. (2005). In "Industrial production and application of carbon nanotubes", company literature Arkema.

Brand, L., Gierliengs, M., Hoffknecht, A., Wagner, V., Zweck. A. (2009). Zukünftige Technologien **79**, 1.

Brandrup, J. (1989). I.E. Polymer Handbook, Jon Wiley & Sons, New York, USA.

Camino, G., Maffezzoli, A., Braglia, M., De Lazzaro, M., Zammarano, M. (2001). Polymer Degradation and Stability **74**, 457.

Capaldi, F.M., Rutledge, G.C., Boyce, M.C. (2005). Macromolecules **38**, 6700.

Caseri, W. (2000). Macromolecular Rapid Communications **21**, 705.

Chang, T.E., Jensen, L.R., Kisliuk, A., Pipes, R.B., Pyrz, R., Sokolov, A.P. (2005). Polymer **46**, 439.

Chen, J., Hamon, M.A., Hu, H., Chen, Y., Rao, A.M., Eklund, P.C., Haddon, R.C. (1998). Science **282**, 95.

Chen, G.X., Shimizu, H. (2008). Polymer **49**, 943.

Coleman, J.N., Khan, U., Blau, W.J., Gunko, Y.K. (2006). Carbon **44**, 1624.

Dreher, K.L. (2004). Toxicological Sciences **77**, 3.

Dresselhaus, M.S., Dresselhaus, G., Avouris, P. (2001). In „Carbon nanotubes: synthesis, structure, properties and application“, Springer, Berlin, Germany.

Dresselhaus, M.S., Dresselhaus, G., Eklund, P.C. (1996). In „Science of fullerenes and carbon nanotubes“, Academic Press, San Diego, USA.

Dumitras, M., Friedrich, C. (2004). Journal of Rheology **48**, 1135.

Esteves, I., Cruz, F., Mueller, E.A., Agnihotri, S., Mota, J.P.C. (2009). Carbon **47**, 948.

Fahrlander, M., Fuchs, K., Friedrich, C. (2000). Journal of Rheology **44**, 1103.

Fasce, D.P., Williams, R.J.J., Mechin, F., Pascault, J.P., Llauro, M.F., Petiaud, R. (1999). Macromolecules **32**, 4757.

Fina, A., Tabuani, D., Frache, A., Camino, G. (2005). Polymer **46**, 7855.

Fukushima, T., Kosaka, A., Ishimura, Y., Yamamoto, T., Takigawa, T., Ishii, N., Aida, T. (2003). Science **300**, 2072.

Ganguly, A., George, J.J., Kar, S., Brandyopadhyay, A., Bhowmick, A.K. (2008). In "Rubber nanocomposites based on miscellaneous nanofillers", Boca Raton, CRC Press, 89.

Ganß, M., Satapathy, B.K., Thunga, M., Weidisch, R., Pötschke, P., Jehnichen, D. (2008). Acta Materialica **56**, 2247.

Gao, C., Muthukrishnan, S., Li, W., Yuan, J., Xu, Y., Muller, H.E. (2007). Macromolecules **40**, 1803.

Geim, A.K., Novoselov, K.S. (2007). Nature Materials **6**, 183.

Gilman, J.W. (1999). Applied Clay Science **15**, 31.

Greßler, S., Fries, R., Simko, M. (2011). Nano trust dossiers **022**, 1.

Gomathi, A., Gopalakrishnan, K., Rao, C.N.R. (2010). Materials Research Bulletin **45**, 1894.

Gozdz, A.S. (1994). Polymer Advanced Technology **5**, 70.

Gyeong-Man, K. (2007). " Verstärkungsmechanismen auf Makro-, Mikro- und Nano-Längenskalen in heterogenen Polymerwerkstoffen", Martin-Luther-Universität Halle-Wittenberg.

Haggenmueller, R., Zhou, W., Fischer, J.E., Winey, K.I. (2003). Journal of Nanoscience and Nanotechnology **3**, 105.

Han, Z., Fina, A. (2011). Progress in Polymer Science **36**, 914.

Hasegawa, N., Okamoto, H., Kato, M., Usuki, A. (2000). Journal of Applied Polymer Science **78**, 1918.

Hermans, P.H., Weidingeer, A. (1961). Macromolecular Chemistry and Physics **44**, 98.

Von Hohenheim, T., von Bodenstein, A. (1572). Paracelsus, Sämtliche Werke, Basel.

Iijima, S. (1991). Nature **354**, 56.

Iijima, S., Ichihashi, T. (1993). Nature **363**, 603.

Inayat, A., Klumpp, M., Schwieger,W. (2011). Applied Clay Science **51**, 452.

Jiang, X., Bin, Y., Kikyotani, N., Matsuo, M. (2006). Polymer **38**, 419.

Karian, H.G. (1999). In „Handbook of Polypropylene and Polypropylene Composites“, (M. Dekker, ed.), New York.

Karger-Kocsis, J. (1999). Polypropylene: An A-Z reference, Kluwer Academic Publishers, Boston, USA.

Kashiwagi, T., Gruke, E., Hilding, J., Groth, K., Harris, R., Awad, W., Douglas, J. (2002). Macromolecular Rapid Communications **23**, 761.

Kashiwagi, T., Harris, R.H., Zhang, X., Briber, R.M., Cipriano, B.H., Raghavan, S.R., Awad, W.H., Shields, J.R. (2004). Polymer **45**, 881.

Kelarakis, A., Yoon, K., Sics, I., Somari, R.H., Chen, X., Hsiao, B.S. (2006). Journal of Macromolecular Science Part B – Physics **45**, 247.

Kiliaris, P., Papaspyrides, C.D. (2010). Progress in Polymer Science **35**, 902.

Kojima, Y., Usuki, A., Kawasumi, M., Okada, A., Fukushima, Y., Kurauchi, T., Kamigaito, O. (1993). Journal of Materials Research **8**, 1185.

Kristiansen, M., Werner, M., Tervoort, T., Smith, P., Blomenhofer, M., Schmidt, H.-W. (2003). Macromolecules **36**, 5150.

Kristiansen, M., Tervoort, T., Smith, P., Goossens, H. (2005). Macromolecules **38**, 10461.

Kuehne, M., Friedrich, C. (2009). Rheologica Acta **48**, 1.

Kuilla, T., Bhadra, S., Yao, D., Kim, N.H., Bose, S., Lee, J.H. (2010). Progress in Polymer Science **35**, 1350.

Lan, Y.-F., Lin, J.-J. (2009). The Journal of Physical Chemistry A **113**, 8654.

LeBaron, P.C., Wang, Z., Pinnavaia, T.J. (1999). Applied Clay Science **15**, 11.

Lee, B.-J. (2009). “Nucleating agent-assisted preparation of polypropylene (PP)/polyhedral oligomeric silsesquioxane (POSS) nanocomposites and their characterization”, Dissertation, The University of Akron.

Lee, C.G., Wei, X.D., Kysar, J.W., Hone, J. (2008). Science **321**, 321.

Lee, Y.-J., Kuo, S.-W., Huang, W.-J., Lee, H.-Y., Chang, F.-C.J. (2004). Journal of Polymer Science Part B: Polymer Physics **42**, 1127.

Lee, S.H., Cho, E.N.R., Jeon, S.H., Youn, J.R. (2007). Carbon **45**, 2810.

Lee, G.W., Jagannathan, S., Chae, H.G., Minus, M.L., Kumar, S. (2008). Polymer **49**, 1831.

Leroux, F., Besse, J.P. (2001). Chemistry of Materials **13**, 3507.

Li, G., Lichang, W., Ni, H., Pittman Jr., C.U. (2001). Journal of Inorganic and Organometallic Polymers **11**, 123.

Lima, M.S.F., Zen Vasconcellos, M.A., Samios, D. (2002). Journal of Polymer Science Part B – Polymer Physics **32**, 896.

Lindberg, H.K., Falck, G.C.M., Suhonen, S., Vippola, M., Vanhala, E., Catalan, J. (2009). Toxicology Letters **186**, 166.

Liu, J., Rinzler, A., Dai, H., Hafner, J.H., Bradley, R.K., Boul, P.J., Lu, A., Iverson, T., Shelimov, K., Huffman, C.B., Fernando, R.M., Shon, Y.S., Lee, T.R., Colbert, D.T., Smalley, R.E. (1998). Science **280**, 1253.

Lopez Manchato, M.A., Valentini, L., Biagiotti, J., Kenny, J.M. (2005). Carbon **43**, 1499.

Luyt, A.S., Dramicanin, M.D., Antic, Z., Djokovic, V. (2009). Polymer Testing **28**, 348.

Ma, H., Tong, L., Xu, Z., Fang, Z. (2007). Nanotechnology **18**, 375602.

Machado, G., Denardin, E.L.G., Kinast, E.J., Goncalves, M.C., de Luca, M.A., Teixeira, S.R., Samios, D. (2005). European Polymer Journal **41**, 129.

Madisons, J. (2011). In „Applications of Polyhedral Oligomeric Silsesquioxanes“, Hartmann-Thompson vol. ed., Springer, Berlin, Germany.

Mantz, R.A., Jones, P.F., Chaffee, K.P., Lichtenhan, J.D., Gilman, J.W., Ismail, I.M.K., Burmeister, M. (1996). Chemistry of Materials **8**, 1250.

Manzi-Nshuti, C., Hossenlopp, J.M., Wilkie, C.A. (2009). Polymer Degradation and Stability **93**, 1855.

Marco, C., Naffakh, M., Gomez, M.A., Santoro, G., Ellis, G. (2011) Polymer Composites **24**, 324.

Marosi, G., Marton, A., Szep, A., Csonto, I., Keszei, S., Zimonyi, E., Toth, A., Alermas, X., Le-Bras, M. (2003). Polymer Engineering and Stability **82**, 379.

Mercurio, D.J., Spontak, R.J. (2001). Journal of Physical Chemistry B **105**, 2091.

McIntosh, D., Khabashesku, V.N., Barrera, E.V. (2006). Chemistry of Materials **18**, 4561.

McIntosh, D., Khabashesku, V.N., Barrera, E.V. (2007). Journal of Physical Chemistry C **111**, 1592.

Meyyappan, M. (2005). In “Carbon nanotubes: science and applications”, Boca Raton, CRC Press.

Mi, Y., Stern, S.A. (1991). Journal of Polymer Science Part B – Polymer Physics **29**, 389.

Mine, T., Komasaki, S. (1985). Japanse Patent Kokai **S 60 210570**.

Mine, T., Komasaki, S. (1985). Japanse Patent Kokai **S 60 210569**.

Mishima, T., Nishimoto, H. (1992). Japanese Patent Kokai **H 4 247405**.

Mishima, T., Nishimoto, H. (1992). Japanese Patent Kokai **H 4 271306**.

Monner, H.P., Mühle, S., Wierach, P., Riemenschneider, J. (2003). Adaptronic Congress 01.-03. April, 1.

Muller, J., Huaux, F., Lison, D. (2006). Carbon **44**, 1048.

Nadella, H.P., Henson, H.M., Spruiell, J.E., White, J.L. (1977). Journal of Applied Polymer Science **21**, 3003.

Noorden, R.V. (2011). Nature **469**, 14.

Nyambo, C., Wilkie, C.A. (2009). Polymer Degradation and Stability **94**, 506.

Nyambo, C., Kandare, E., Wilkie, C.A. (2009). Polymer Degradation and Stability **94**, 513.

Ogino, S., Sato, Y., Yamamoti, G., Sasamori, K., Kimura, H., Hashida, T., Motomiya, K., Jeyadevan, B., Tohji, K.J. (2006). The Journal of Physical Chemistry B **110**, 23159.

Onder, E., Sarier, N., Ersoy, M.S. (2012). Thermochimica Acta **543**, 37.

Pavlidou, S., Papasyrides, C.D. (2008). Progress in Polymer Science **33**, 12.

Paracelsus, A.T., von Bodenstein, A. (1563). Paracelsus, Sämtliche Werke, Basel.

Peigney, A., Laurent, C., Flahaut, E., Basca, R.R., Rousset, A. (2001) Carbon **39**, 507.

Peng, H., Alemany, L.B., Margrave, J.L., Khabeshesku, V.N. (2003). Journal of the American Chemical Society **125**, 15174.

Perilla, J.E., Lee, B.-J., Jana, S.C. (2010). Journal of Rheology **54**, 761.

Prashantha, K., Soulestin, J., Lacrampe, M.F., Krawczak, P., Dupin, G., Claes, M. (2009). Composite Science and Technology **69**, 1756.

Prashantha, K., Soulestin, J., Lacrampe, M.F., Claes, M., Dupin, G., Krawszak, P. (2008). Polymer Letters **2**, 735.

Price, B.K., Hudson, J.L., Tour, J.M. (2005). Journal of the American Chemical Society **127**, 14867.

Ray, S.S. (2006). Journal Indian Engineering Chemistry **12,** 811.

Ray, S.S., Okamoto, M. (2003). Progress in Polymer Science **28**, 1539.

Rives, V. (2001). In “Layered double hydroxides – present and future”, Nova Science Publishers Inc., New York, USA, 285.

Robertson, J. (2004). Materials Today **7**, 46.

Roy, S., Scionti, V., Jana, S.C., Wesdemiotis, C., Pischera, A.M., Espe, M.P. (2011). Macromolecules **44**, 8064.

Roy, S., Lee, B.J., Kakish, Z.M., Jana, S.C. (2012). Macromolecules **45**, 2420.

(b) Roy, S., Feng, J., Scionti, V., Jana, S.C., Wesdemiotis, C. (2012). Polymer **53**, 1711.

Roy, N., Sengupta, R., Bhowmick, A.K. (2012). Progress in Polymer Science **37**, 781.

Saito, Y., Tsuchiya, M., Itoh, Y. (1983). Japanese Patent Kokai **S 58 14928**.

Saito, R., Fujita, M., Dresselhaus, G., Dresselhaus, M.S. (1992). Applied Physics Letters **60**, 2204.

Sandler, J., Shaffer, M.S.P., Prasse, T., Bauhofer, W., Schulter, K., Windle, A.H. (1999). Polymer **40**, 5967.

Sandler, J., Broza, G., Nolte, M., Schulter, K., Lam, Y.M., Shaffer, M.S.P. (2003). Journal of Macromolecular Science – Physics **42**, 479.

Schartel, B., Pötschke, P., Knoll, U., Goad, M.A. (2005). European Polymer Journal **41**, 1061.

Scott, T.K., Jack, F.D., Francis, W.S. (2007). Journal of Polymer Science Part B: Polymer Physics **45**, 1882.

Scott, D.W. (1946). Journal of the American Chemical Society **68**, 356.

Sellinger, A., Laine, R.M. (1996). Macromolecules **29**, 2327.

Shanmugharaj, A.M., Bai, J.H., Nayak, R.R., Ryu, S.H. (2007). Journal of Polymer Science Part A: Polymer Chemistry **45**, 460.

Shepard, C.U., Still, J. (1835). American Journal of Science and Arts **28**, 145.

Shepar, T.A., Delsorbo, C.R., Louth, R.M., Walborn, J.L., Norman, D.A., Harvey, N.G., Spontak, R.J. (1997). Journal of Polymer Science Part B: Polymer Physics **35**, 2617.

Shi, D., Lian, J., He, P., Wang, L.M., Xiao, F., Yang, L., Schultz, M.J., Mast, D.B. (2003). Applied Physics Letters **83**, 5301.

Shoji, F., Sudo, R., Watanabe, T. (1981). Japanese Patent Kokai S 56 146120.

Singh, V., Joung, D., Zhai, L., Das, S., Khondaker, S.I., Seal, S. (2011). Progress in Materials Science **56**, 1178.

Socher, R., Krause, B., Müller, M.T., Boldt, R., Pötschke, P. (2012). Polymer **53**, 495.

Arvidson, S.A., Khan, S.A., Gorga, R.E. (2012) Macromolecules **43**, 2916.

Song, P., Cao, Z., Cai, Y., Zhao, L., Fang, Z., Fu, S. (2011). Polymer **52**, 4001.

Stein, R.S. (1958). Journal of Polymer Science **31**, 327.

Theng, B.K.G. (1974). In “The chemistry of clay-organic reactions”, Adam Hilger Ltd.

Thierry, A., Fillon, B., Straupe, C., Lotz, B., Wittmann, J.C. (1992). Progress in Colloid and Polymer Science **87**, 28.

Thostenson, E.T., Ren, Z., Chou, T.-W. (2001). Composites Science and Technology **61**, 1899.

Tjong, S.C., Liang, G.D., Bao, S.P. (2007). Scripta Materialia **57**, 461.

Trifiro, F., Vaccari, A. (1996). Supramolecular Chemistry **7**, 251.

Tsutsui, M., Kato, S. (1988). Japanese Patent Kokoku **S 63 20210**.

Qian, D., Dickey, E.C., Andrews, R., Rantell, T. (2000). Applied Physics Letters **76**, 2868.

Uchimura, S., Sato, M., Makino, D. (1983). Japanese Patent Kokai **S 58 96654**.

Usuki, A., Kojima, Y., Kawasumi, M., Okada, A., Fukushima, Y., Kurauchi, T., Kamigaito, O. (1993). Journal of Materials Research **8**, 5.

Usuki, A., Koiwai, A., Kojima, Y., Kawasumi, M., Okada, A., Kurauchi, T., Kaimigaito, O. (1995). Journal of Applied Polymer Science **55**, 1.

Vaisman, L., Marom, G., Wagner, H.D. (2006). Advanced Functional Materials **16**, 357.

Valentino, O., Sarno, M., Rainone, N.G., Nobile, M.R., Ciambelli, P., Neitzert, H.C., Simon, G.P. (2008). Physica E: low-dimensional systems and Nanostructures **40**, 2440.

Valentinus, B., Naumann, J., Wolff, G. (1677). Das Vierdte Buch, Hamburg.

Vargas, A.F., Orozco, V.H., Rault, F., Giraud, S., Debauc, E., Lopez, B.L. (2010). Composites: Part A **41**, 1797.

Vlasveld, D.P.N., de Jong, M., Bersee, H.E.N., Gotsis, A.D., Picken, S.J. (2005). Polymer **46**, 10279.

Wagner, R., Reisinger, T.J.G. (2003). Polymer **44,** 7513.

Wang, D.-Y., Leuteritz, A., Kutlu, B., Auf der Landwehr, M., Jehnichen, D., Wagenknecht, U., Heinrich, G. (2011). Journal of Alloys and Compounds **509**, 3497.

Wilchinsky, Z.W. (1963). In “Advances in X-ray Analysis”, Plenum Press **6**, New York.

Wilchinsky, Z.W. (1960). Journal of Applied Physics **31**, 1969.

Wilchinsky, Z.W. (1959). Journal of Applied Physics **30**, 792.

Williams, K.A., Veenhuizen, T.M., Torre, G., Eritja, R., Dekker, C. (2002). Nature **420**, 761.

Wu, J., Mather, P.T. (2009). Polymer Reviews **49**, 25.

Xia, H.S., Wang, Q., Li, K.S., Hu, G.H. (2004). Journal of Applied Polymer Science **93**, 378.

Xiao, Y., Zhang, X., Cao, W., Wang, K., Tan, H., Zhang, Q. (2007). Journal of Applied Polymer Science **104**, 1880.

Xu, M., Zhang, T., Gu, B., Wu, J., Chen, Q. (2006). Macromolecules **39**, 354.

Yanagisawa, M. (1987). Japanese Patent Kokai **S 62 89228**.

Yoneda, Y., Kitamura, T., Naito, J., Kitakohji, T. (1982). Japanese Patent Kokai **S 57 168246**.

Yoneda, Y., Takeda, S., Kitamura, T., Nakajina, M., Kitakohiji,T. (1982). Japanese Patent Kokai **S 57 168247**.

Zanetti, M., Camino, G., Mühlhaupt, R. (2001). Polymer Degradation and Stability **74**, 413.

Zhang, Y., Ali, S.F., Dervishi, E., Xu, Y., Li, Z., Casciano, D. (2010). ACS Nano **4**, 3181.

Zhang, B., Chen, Y., Wang, J., Blau, W.J., Zhuang, X., He, N. (2010). Carbon **48**, 1738.

Zhao, Y., Schiraldi, D.A. (2005). Polymer **46**, 11640.

Zheng, L., Waddon, A.J., Farris, R.J., Coughlin, E.B. (2002). Macromolecules **35**, 2375.

Zhou, X., Xie, X., Zeng, F., Li, R., Mai, Y.W. (2006). Key Engineering Materials **312**, 223.

Zhou, Z., Wang, S., Lu, L., Zhang,Y., Zhang, Y. (2007). Journal of Polymer Science Part B – Polymer Physics **45**, 1616.

Zhu, J., Uhl, F.M., Morgan, A.B., Wilkie, C.A. (2001). Chemistry of Materials **13**, 4649.